Analysis and design of two-way slabs strengthened in flexure with FRCM

Majid M.A. Kadhim [a], Akram Jawdhari [b,*], Ali Hadi Adheem [c], Amir Fam [d]

[a] University of Babylon, Hilla, Iraq
[b] Valparaiso University, Valparaiso, IN 46384, USA
[c] Kerbala Technical Institute, Al-Furat Al-Awsat Technical University, 56001 Kerbala, Iraq
[d] Queen's University, Kingston, ON K7L 3N6, Canada

ARTICLE INFO

ABSTRACT

Fabric reinforced cementitious mortar (FRCM), an emerging sustainable retrofit technique, has seen very limited research and applications on two-way reinforced concrete (RC) slabs. In this study, a three-dimensional finite element (FE) model is developed for FRCM-strengthened slabs, incorporating concrete nonlinearity, cracking, debonding and rupture. After validation with experimental results from literature, an extensive parametric study was performed, examining the effects of FRCM coverage area as a ratio of the width of FRCM reinforcement (w_{FRCM})-to-span (S); the use of discontinuous FRCM strips; internal steel reinforcement ratio (ρ_s); compressive strength of concrete (f'_c); and aspect ratio of slab (α). The study showed that ultimate strength (P_u) increases sharply by 84% as (w_{FRCM}/S) increased from zero to 0.25, then only by 19% from (w_{FRCM}/S) of 0.25 to 1.0. In general, P_u increased with f'_c and ρ_s but was not affected by α. Two existing models were evaluated and found to be unconservative or insensitive to key parameters. A regression analysis was performed on data from the parametric study, resulting in two expressions for the FRCM effective strain (ε_{fe}) and much better predictions for P_u.

1. Introduction

Modern repair and strengthening methods of concrete structures due to aging, environmental-induced deterioration, increase in loads, compliance with new codes or extreme load events, have involved fiber reinforced polymer (FRP) composites [1–3]. FRPs offer high strength to weight ratio, resistance to corrosion, ease of handling and installation, and good fatigue performance [2–5]. Several systems have been developed, including externally bonded (EB) plates or sheets [6,7], externally bonded reinforcement in grooves (EMBROG) [8], near-surface mounted (NSM) rods or strips [3,9–11], and rod panels [4,12–14]. Typically, the FRP reinforcement is attached to the surface by a high-strength organic adhesive such as epoxy [2].

Although proven to be successful in rehabilitating various materials such as concrete, steel, and masonry [1,2,15–18], under various loading conditions including flexure, shear, axial and torsion [3–5,11], epoxy-bonded FRP systems have a number of limitations, including their poor behavior at elevated temperatures and under fire, inapplicability on wet surfaces or at low temperatures and lack of vapor permeability and irreversibility [19–22]. Furthermore, handling epoxy materials during installation or inhaling their residues during fire events could

also pose a health hazard due to their toxic nature [22]. A recent technique, comprising fabrics and open meshes of dry fibers embedded in cement-based inorganic matrices, has been developed to overcome the above limitations [18–20,23]. The fibers can be carbon, glass, basalt, polyparaphenenylene benzobisoxazole (PBO), steel, polymeric, or a combination of multiple types [23]. Although mostly known as fabric-reinforced cementitious matrix (FRCM), the system is also referred to as textile reinforced mortar (TRM) and mineral based composite (MBC) [24].

Research on FRCM has increased steeply in the last two decades, with great results for concrete structures [20,25], including enhancing strength and stiffness as well as improving the behavior under elevated temperatures or in fire [22,24–28]. For examples, Ombres [29] tested 12 RC beams strengthened in flexure with PBO-FRCM and reported 10 to 44% increase in ultimate load. Alabdulhady, Sneed [27] also used PBO-FRCM to strengthen RC rectangular beams for torsion and reported increases in cracking torque, torsional strength, and twist when 4-sided jackets are applied. FRCM jackets have been used to wrap concrete columns, and resulted in a comparable (80–90%) confinement effectiveness, compared to FRP [30,31]. The system was also successfully deployed for masonry walls, where it increased load capacity and

---

Table 1
FE predictions of key results and comparisons with test data.

Specimen ID	Ultimate load, P_u (kN)			Central deflection at P_u (mm)			Cracking load (kN)		
	Exp.	FE	FE/ Exp.	Exp.	FE	FE/ Exp.	Exp.	FE	FE/ Exp.
CON[1]	95	95	1.00	52	47	0.90	40	40	1.00
C1[2]	207	209	1.01	37	34	0.92	70	77	1.10
C2[3]	291	297	1.02	35	38	1.09	90	92	1.02
C1-part[4]	178	189	1.06	25	27	1.08	75	80	1.07

[1] Control, no strengthening.
[2] Strengthened with one, full-length FRCM layer.
[3] Strengthened with two, full-length FRCM layers.
[4] Strengthened with two, half-length FRCM layers.

deformability [32–34].

While ample research was conducted on beams, walls and columns, fewer studies were focused on slabs, particularly two-way ones [35]. Of those available, Loreto, Leardini [36] tested 12 FRCM-strengthened one-way slabs with dimensions of 1829 × 305 × 152 mm under four-point bending. The FRCM system resulted in 141 and 205% increase in ultimate load for slabs having a f'_c of 28 MPa and strengthened with one and four FRCM layers, respectively; and 135 and 212% for slabs with a f'_c of 40 MPa and same respective number of plies. Aljazaeri and Myers [20] also tested one-way slabs in flexure and compared the effectiveness of PBO-FRCM system with two epoxy-bonded ones, namely Carbon-FRP (CFRP) grid and steel-reinforced polymer (SRP) wire mesh. FRCM was found to provide higher ultimate loads than CFRP grid and much better ductility.

Only three studies could be found in the open literature where FRCM is used to strengthen two-way slabs. Papanicolaou, Triantafillou [37] tested four slabs measuring 2000 × 2000 × 120 mm under monotonic flexural load to failure. The slabs were cast with edge beams, simply supported, and were strengthened with either one and two layers of carbon-FRCM (C-FRCM) or 3 layers of glass-FRCM (G-FRCM). The ultimate load was increased by 26 to 53%, with higher stiffness and better energy absorption. Koutas and Bournas [35] conducted flexural tests on six half-scale two-way slabs, with dimensions 1800 × 1800 × 100 mm. Strengthening with C-and G-FRCM layers proved to be effective where it resulted in increasing the pre- and post-cracking stiffness, cracking and ultimate loads. Further details into these tests, which are used as a baseline to validate and calibrate the three-dimensional finite element model developed in this study are presented later. The third study investigated the flexural response of two-way slabs with cut openings strengthened with FRCM composites [38]. The examined parameters included the number of FRCM layers, textile type, the strengthening configuration, and the matrix material. It was found that the FRCM technique is able to restore the flexural capacity of two-way slabs with openings.

While the FRCM technique has become increasingly studied and used, its application on two-way RC slabs remains very limited. This study aims to fill this gap and ultimately provide a reliable design tool for flexural strengthening of two-way slabs using FRCM. To achieve this, a robust three-dimensional finite element (FE) model is developed and validated using a recent experimental study from literature. The model was then used in a comprehensive parametric study. Based on regression analysis of the results, a simplified design equation is presented for the moment capacity of two-way RC slabs strengthened by FRCM system.

2. Summary of experiments

Results of the experimental study conducted by Koutas and Bournas [35] on two-way RC slabs tested under monotonic flexure is used to validate the numerical model (Table 1). Four slabs were selected for modeling and were simply supported at their perimeter and loaded at four central points, spaced at 500 mm (Fig. 1). The slabs had an aspect ratio of 1.0, with total and effective spans of 1.8 and 1.5 m, respectively, and a thickness of 100 mm. They were under-reinforced, with an

intentionally reduced reinforcement ratio (ρ_s) of 0.17%, to simulate a need for repair stemming from steel corrosion or an overloading. The bottom face of mid-span region was reinforced with 6 mm-diameter plain rebars spaced at 200 mm (Fig. 2(a)). One half of the reinforcement continued over the support region, but the other half was bent and used as a top reinforcement. At the corners which may experience twisting moments and concrete cracking, a grid of 8-mm deformed bars was added at the top face. Moreover, the perimeter was also reinforced with two 8 mm deformed bars located on either the bottom or top faces (Fig. 2 (a)).

One slab (CON) was un-strengthened and served as a baseline to evaluate the effectiveness of FRCM system. Slabs C1 and C2, respectively, were strengthened with one and two layers of carbon-FRCM (C-FRCM) covering the entire bottom face (Fig. 3). Slab C1-part was strengthened with two orthogonal strips of C-FRCM system with each strip covering half the width of the respective side (Fig. 1). While the textile in slabs C1 and C2 consisted of several segments made continuous by overlapping, it was modeled numerically as one continuous layer because the overlaps were located at low stress regions and didn't debond experimentally. The application of FRCM reinforcement followed the typical procedure employed for beams and other elements and started by scarifying the concrete face to enhance bond, moistening the concrete surface, applying the first 2 mm-thick mortar coat, laying and pressing the carbon textile, and covering with a final mortar coat, also 2 mm thick. The authors conducted ancillary material tests and reported values of 19.8 to 22.2 MPa for the compressive strength of concrete; 33.1 to 36.6 MPa for the compressive strength of mortar; 470 and 508 MPa for the yield and ultimate strengths, respectively, of the 6 mm plain rebars; and 568 and 654 for the same respective strengths of the 8 mm deformed bars. The modulus of elasticity and the tensile strength of the carbon textile were reported by the manufacturer to be 225 GPa and 3800 MPa, respectively. The textile weighed 348 g/m^{3} and contained uncoated (dry) carbon-fiber rovings, distributed equally in two orthogonal directions and spaced centrally at 10 mm.

The study showed that FRCM was very effective for two-way slabs where strengthening with one and two layers of full-length C-FRCM reinforcement resulted in 115 and 206%, respectively, increase in flexural capacity. Strengthening with two half-width orthogonal layers was less effective than one continuous layer, yet provided an 87% increase. Specimens CON, C1 and C1-part failed by flexure while C2 by punching shear. In the strengthened slabs, the C-FRCM textile also experienced slipping from mortar and sometimes partial rupture. Further improvement due to strengthening was also reported for cracking load, the pre- and post-cracking stiffness.

3. Finte element model

The slab models were generated in ABAQUS software [39] using its explicit dynamics solver in lieu of the implicit static solver, which is oftentimes difficult to converge, particularly for problems with high nonlinearities or with contacts [39]. The inertial forces that sometimes exist in transient analyses were minimized by using a large analysis time and applying the load as a constant velocity. A quarter-size model was
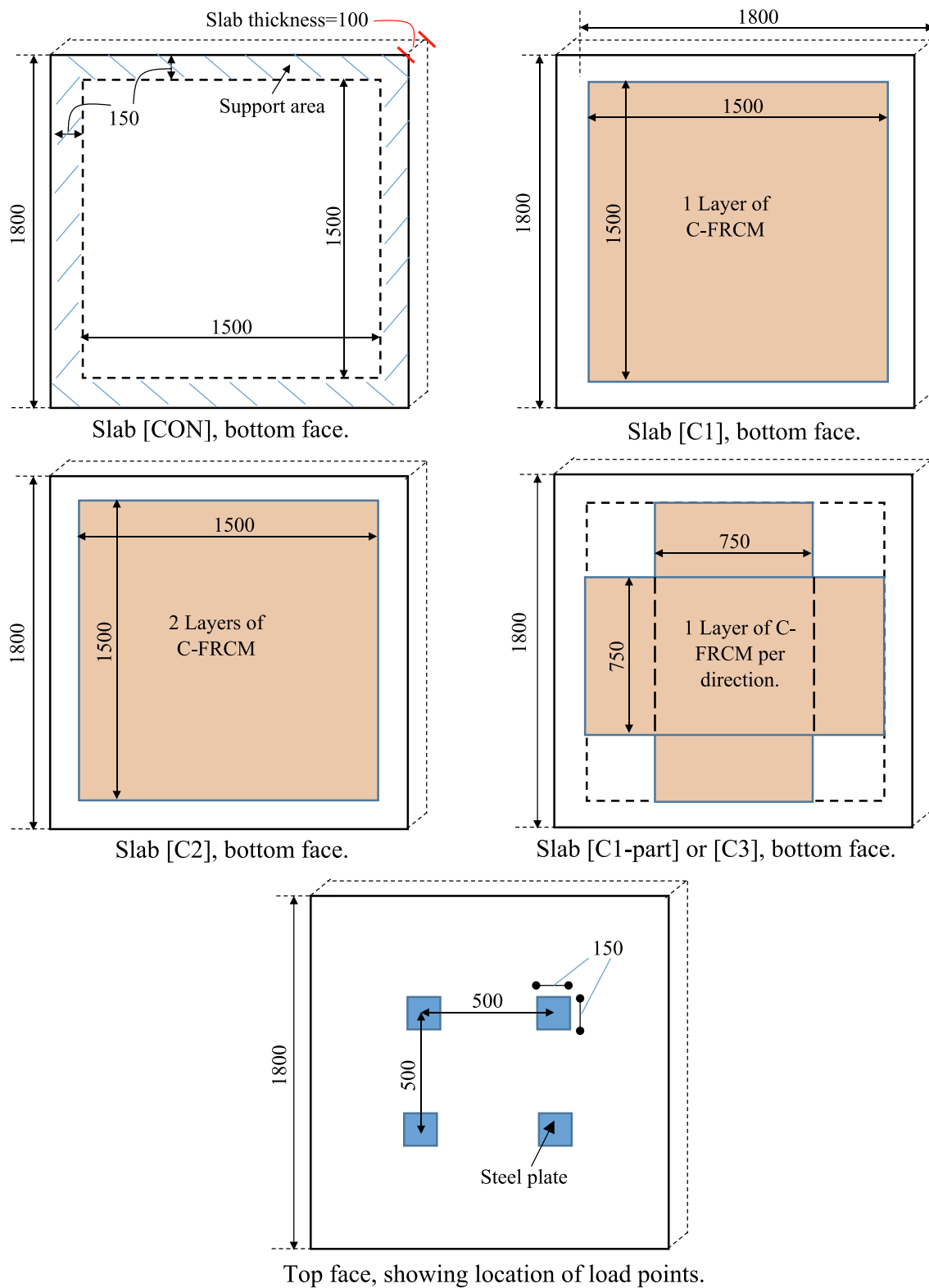
Slab [CON], bottom face.

Slab [C1], bottom face.

Slab [C2], bottom face.

Slab [C1-part] or [C3], bottom face.

Top face, showing location of load points.

Fig. 1. FRCM strengthening configuration and loading scheme for slabs tested by [35].

used, benefiting from symmetry in materials and geometry, to reduce run time and desk space (Fig. 2(b)). At each plane of symmetry, proper restraints were given to translational and rotational displacements. The concrete volume, mortar layers, and steel plates at loading and support were modeled by an 8-noded brick elements (C3D8R) with reduced integration algorithm. The steel reinforcement and fabric were modeled by 2-noded truss elements (T3D2) and 4-noded shell elements (S4R), respectively.

Because textile slipping from mortar was predominant in the slab tests as reported in [35] and also in numerous studies deploying FRCM as a strengthening system, it was imperative to accurately model the textile-mortar interface and include a bond-slip relation. The contact
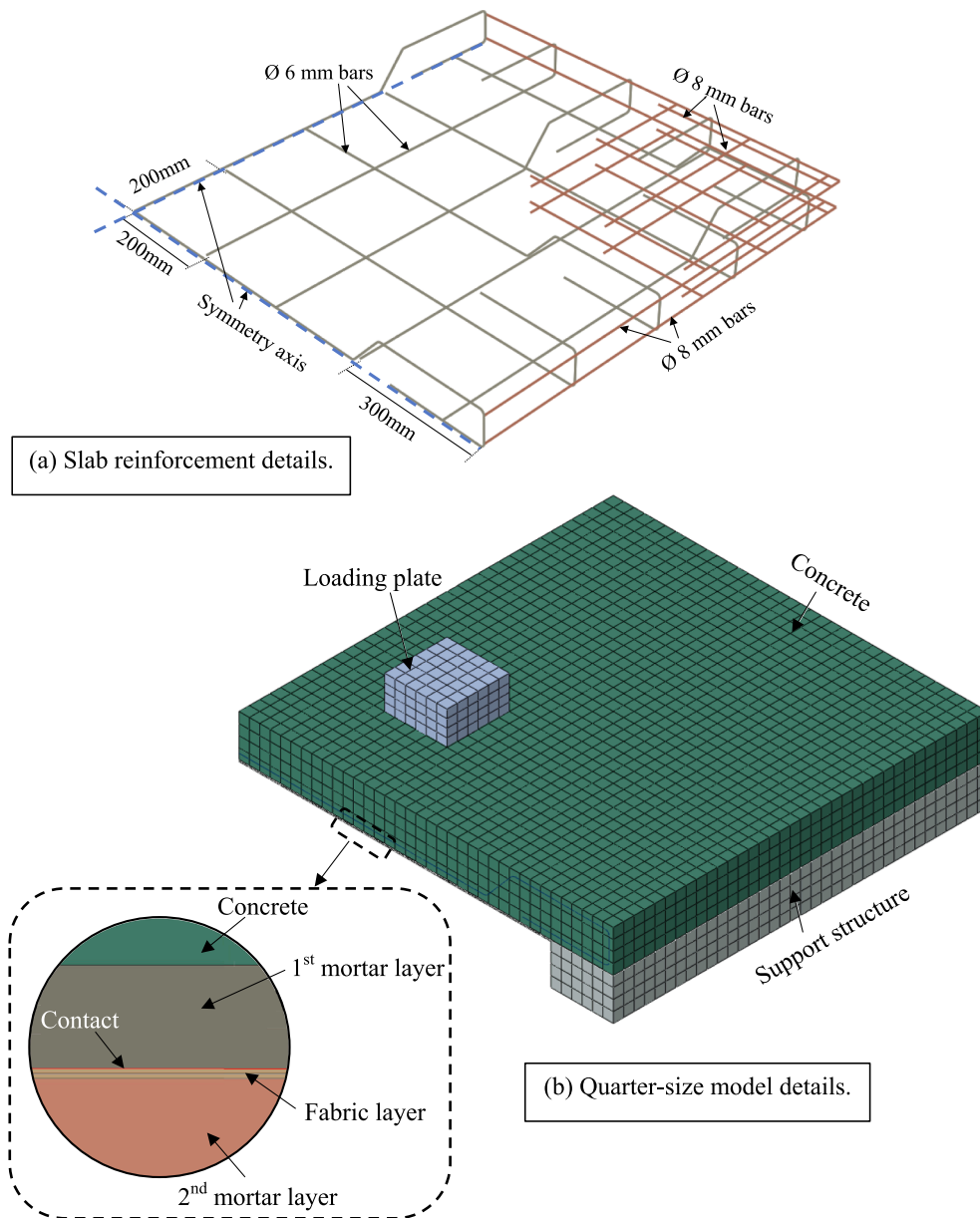
(a) Slab reinforcement details.

(b) Quarter-size model details.

Fig. 2. Finite element model for FRCM-strengthened two-way RC slabs.

surface was modeled by cohesive elements (COH3D8) which are frequently used to model bonded joints such as between concrete and FRP [6] or steel and FRP [40,41]. The interfacial bond-slip relation for the textile-mortar interface is discussed separately later. The steel reinforcement was assumed to be perfectly bonded to concrete and was simulated in the model by using embedded reinforced method available in ABAQUS [6,42]. Although the bond between the 6 mm plain rebars and concrete slab is expected to result in some slipping, a perfect bond assumption was adopted because the rebars had 180° end-hooks and were not reported in the experimental study by Koutas and Bournas [35] to deboned or slip. A mesh sensitivity study was conducted on the control slab to select an optimum element size that provides an accurate result but with minimum computing efforts. A mesh with an element side length of 25 mm was found sufficient for the above objective and as an example, it resulted in a total number of elements of 8230 for slab CON and 13,234 for slab C2.

3.1. Material modelling

Concrete: the concrete damage plasticity (CDP) is the hallmark of ABAQUS constitutive laws for brittle materials and was used in this study to model the concrete and mortar parts. CDP requires defining several inputs to accurately simulate the nonlinear behavior of concrete-like materials, including: the compressive strength (f'_c), modulus of elasticity (E), Poisson's ratio (v), dilation angle (ψ), shape factor (K_c), stress ratio (σ_{bo}/σ_{co}) and eccentricity (ε). E of concrete was estimated from the American Concrete Institute (ACI) theoretical formula of ($E = 4700\sqrt{f'_c}$) [43], and v_c taken as 0.2 [6,28]. Typical values of $\psi = 40°$, $K_c = 0.667$, $\sigma_{bo}/\sigma_{co} = 1.16$, and $\varepsilon = 0.1$, were assumed for the other parameters based on the recommendations of several studies [6,44].

The CDP also requires defining the stress-strain response in compression and tension. The model by Kent and Park (K&P) [45] was used to model the compressive behavior, where the response is assumed to be linear for stresses up to $0.5f'_c$, and nonlinear until it reaches the compressive strength (f'_c), as can be seen in Fig. 3. Post f'_c, the curve
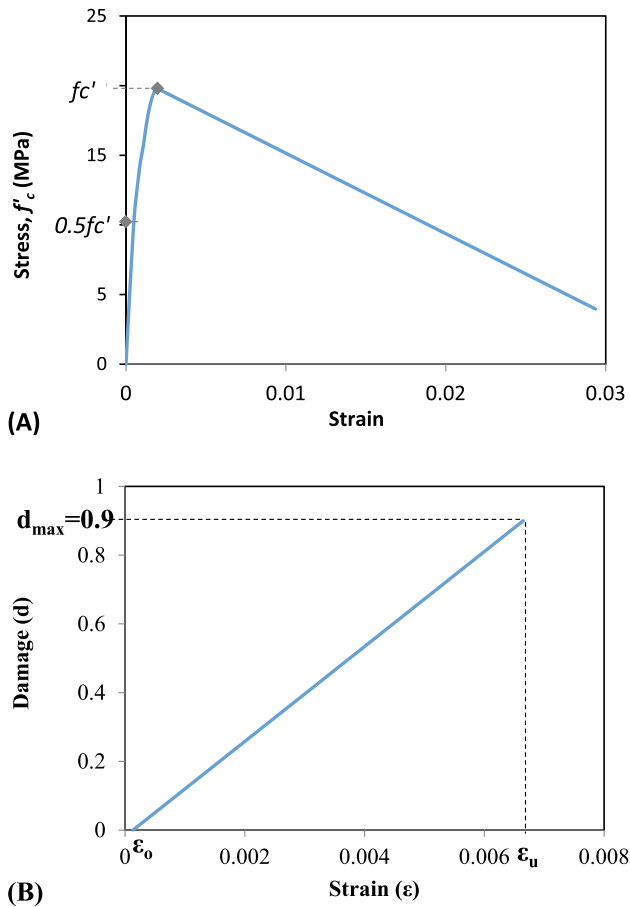
Fig. 3. Concrete material modeling, (A) compressive behavior; (B) damage parameter- tensile strain relationship.
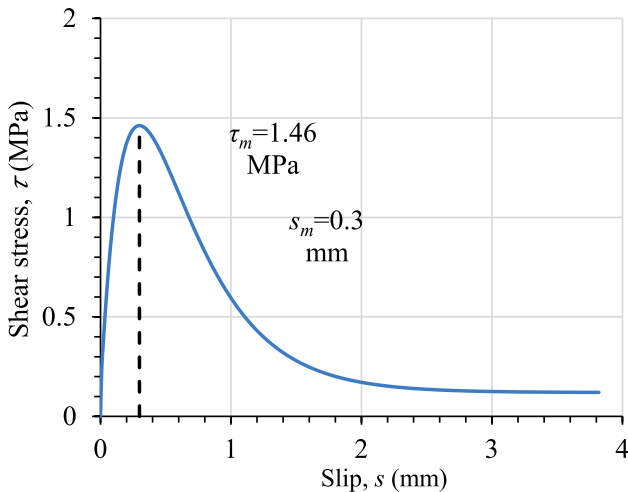

Fig. 4. Shear stress versus slip relationship for textile-mortar interface.

descends linearly at a slope dependent on the confinement from shear reinforcement, and then plateaus at a stress of $0.2f'_c$. Further details about theoretical formulations and applications of K&P model can be found in [4,45]. The tensile stress-strain is modelled as linear elastic until the tensile strength (f_t) of concrete or mortar is reached, and then descends linearly to a stress of zero at a strain of 50 times that accompanying f_t. [42]. The tensile damage parameter (d_t) is activated to represent the descending part of the stress-strain curve in tension,

according to Eq. (1):

$$d_t = 1 - \frac{\sigma_t}{f_t} \tag{1}$$

where the value of d_t should be between 0 and 1 for uncracked and cracked elements, respectively, but preferably slightly less than 1 for cracked stage to avoid numerical problems [6]. In this study, d_t is taken as 0.9 for fully cracked elements, as can be seen in Fig. 3.

Steel: the steel sections used to simulate loading and supports were modeled as linear elastic, using typical values of 200 GPa and 0.3 for the elastic modulus (E_s) and Poison's ratio (v_s), respectively. An elastic-plastic (E-P) model was deployed to model the slab's steel reinforcement and to simulate its yielding and rupture failures. Aside from E_s and v_s, which are assumed to be equal to those for loading and support sections, the yield and ultimate strengths were also defined for the E-P model, using the values reported earlier for the 6 mm plain and 8 mm deformed bars.

Textile: the textile used in the experimental study by Koutas and Bournas [35] to form the C-FRCM system consists of an open grid of carbon fiber strands distributed equally in two orthogonal directions. In the model, the grid was converted into an orthogonal solid plate by smearing the strands area into an equivalent thickness, and molded by shell element using the composite layup section available in ABAQUS [39]. The major material inputs required to define the elastic behavior and brittle failure of the textile in each layer are: elastic modulus (E_f), Poison's ratio (v_{12}), shear modulus (G_{12}), and tensile strength (σ_f). Aside from E_f and σ_f, which are taken from [35] and reported earlier, v_{12} and G_{12}, are assumed to be 0.28 and 5500 MPa, respectively, following the recommendations of [6,28].

3.2. Interface modeling

Although debonding of FRCM can practically occur at either the interface between concrete and mortar layer, or between mortar and fabric, numerous studies showed that the latter interface debonding is more prevalent than the former [46,47]. The textile-mortar debonding is a ductile type [35] characterized by slippage of fiber bundles from the embedding matrix, and is not affected by the mechanical properties of the concrete substrate [48]. Mostly, a pure shear (Mode-II) interfacial bond-slip (τ-s) relation or facture mechanics approach are used to simulate the textile debonding phenomenon [10].

In this study, the bond-slip model suggested by Zou, Sneed [47] is used to represent the fiber slipping from mortar for the two-way slabs strengthened by FRCM. The model is characterized by three parts, a linear increasing one until the maximum shear (bond) strength (τ_m) is reached at a slip (s_m), then a nonlinear decreasing one, and final part representing a constant shear stress associated with friction (matrix-fiber interlocking) (Fig. 4). Equations (2) and (3) can be used to determine the numerical values for τ_m and s_m, respectively;

$$\tau_m = \frac{A^2 B E_f t_f}{4} + \tau_f \tag{2}$$

$$s_m = 0.693/B \tag{3}$$

where A and B are empirical parameters found by Zou, Sneed [47] to be 0.0104 and 2.32 mm^{-1} respectively; E_f and t_f are the elastic modulus and thickness of textile; τ_f is shear stress due to friction and interlocking and is equal to 0.08–0.12 MPa based on recommendations of Carloni, D'Antino [49], with the value of 0.12 MPa selected in this study. Fig. 4 shows a typical τ-s relation with numerical values for the slabs tested in Koutas and Bournas [35]. This relation was defined at the interface between the mortar and textile, while that between mortar and concrete substrate was treated as perfectly bonded.

The τ-s relation in Fig. 4 was implemented in ABAQUS using the traction-separation model, which is based on three components, initial

Table 2
Description and key results, sample of 22 slab models constructed for parametric analysis.

Specimen ID	Studied Variable					Ultimate load, P_u (kN)	Control case	P_u /$P_{u\text{-}control}$
	Description	Symbol	Unit		Value			
FE- SP1	FRCM coverage area	W_{FRCM} /S	Ratio		0.25	175.0	Slab C1	0.84
FE- SP2					0.75	204.6		0.98
FE- SP3	No. of discontinuous FRCM strips	N	Number		3	187.1	Slab C3	0.99
FE- SP4					5	182.6		0.97
FE- SP5[1]	Steel reinforcement ratio	ρ_s	Ratio		0.0035	235.2	Slab C1	1.13
FE- SP6[1]					0.0070	302.6		1.45
FE- SP7[1]					0.0130	365.5		1.75
FE- SP8[2]					0.0035	218.6	Slab C3	1.16
FE- SP9[2]					0.0070	295.7		1.57
FE- SP10[2]					0.0130	346.9		1.84
FE- SP11[1]	Concrete compressive strength	f'_c	MPa		15	188.3	Slab C1	0.91
FE- SP12[1]					30	239.7		1.15
FE- SP13[1]					40	260.4		1.25
FE- SP14[2]					15	174.5	Slab C3	0.93
FE- SP15[2]					30	222.8		1.18
FE- SP16[2]					40	249.5		1.33
FE- SP17[3]	Slab's aspect ratio	α	Ratio		1.25	204.0	Slab C1	0.98
FE- SP18[3]					1.50	214.3		1.03
FE- SP19[3]					1.75	218.1		1.05
FE- SP20[4]					1.25	196.1	Slab C3	1.04
FE- SP21[4]					1.50	182.0		0.97
FE- SP22[4]					1.75	177.5		0.94

[1] Slab is strengthened by one FRCM layer covering the entire tensile face, W_{FRCM} /S = 1.0.
[2] Slab is strengthened by two orthogonal FRCM layers, each with a width of half the span, W_{FRCM} /S = 0.5.
[3] Slab is strengthened by one FRCM layer covering the entire tensile face, W_{FRCM} /S = 1.0. In addition, ρ_s = 0.0017.
[4] Slab is strengthened by two orthogonal FRCM layers, each with a width of half the span, W_{FRCM} /S = 0.5. In addition, ρ_s = 0.0017.

Specimen ID	Studied Variable						Ultimate load, P_u (kN)	Control case	P_u /$P_{u\text{-}control}$
	ρ_s	W_{FRCM} /S	n	N	f'_c	α			
FE- SP1	0.0017	0.25	2	1	20	1.00	175.0	Slab C1	0.84
FE- SP2	0.0017	0.75	2	1	20	1.00	204.6		0.98
FE- SP3	0.0017	0.50	2	3	20	1.00	187.1	Slab C3	0.99
FE- SP4	0.0017	0.50	2	5	20	1.00	182.6		0.97
FE- SP5	0.0035	1.00	1	1	20	1.00	235.2	Slab C1	1.13
FE- SP6	0.0070	1.00	1	1	20	1.00	302.6		1.45
FE- SP7	0.0130	1.00	1	1	20	1.00	365.5		1.75
FE- SP8	0.0035	0.50	2	1	20	1.00	218.6	Slab C3	1.16
FE- SP9	0.0070	0.50	2	1	20	1.00	295.7		1.57
FE- SP10	0.0130	0.50	2	1	20	1.00	346.9		1.84
FE- SP11	0.0017	1.00	1	1	15	1.00	188.3	Slab C1	0.91
FE- SP12	0.0017	1.00	1	1	30	1.00	239.7		1.15
FE- SP13	0.0017	1.00	1	1	40	1.00	260.4		1.25
FE- SP14	0.0017	0.50	2	1	15	1.00	174.5	Slab C3	0.93
FE- SP15	0.0017	0.50	2	1	30	1.00	222.8		1.18
FE- SP16	0.0017	0.50	2	1	40	1.00	249.5		1.33
FE- SP17	0.0017	1.00	1	1	20	1.25	204.0	Slab C1	0.98
FE- SP18	0.0017	1.00	1	1	20	1.50	214.3		1.03
FE- SP19	0.0017	1.00	1	1	20	1.75	218.1		1.05
FE- SP20	0.0017	0.50	2	1	20	1.25	196.1	Slab C3	1.04
FE- SP21	0.0017	0.50	2	1	20	1.50	182.0		0.97
FE- SP22	0.0017	0.50	2	1	20	1.75	177.5		0.94

ρ_s: Steel reinforcement ratio; W_{FRCM} /S: width of FRCM layer/ slab width; n: number of FRCM layers (1 means one layer and 2 means two orthogonal FRCM layers; :number of FRCM strips in each direction; f'_c: concrete compressive strength; α: aspect ratio of slab.

response, damage initiation, and damage evolution. The damage initiation is activated by defining τ_m and s_m values, while the initial response is taken as the slope (τ_m/s_m) of the shear stress-slip curve. The debonding process is assumed to start when the interface shear stress (τ) exceeds (τ_m) as defined in the damage initiation criteria. A damage evolution law is used to define the decrease in bond stresses after reaching τ_m and degrade the joint interfacial stiffness. Equation (4) presents the damage evolution parameter (d_m) used by ABAQUS for damage evolution and shows that damage is dependent on current slip (s), slip accompanying τ_m (s_m), and slip at complete debonding (s_f). It should be noted that d_m can have values ranging between 0 [undamaged] and 1.0 [debonded], with intermediate values referring to joints that are damaged but not completely debonded.

$$d_m = 1 - \frac{(s_f - s)}{(s_f - s_m)} \tag{4}$$

4. Validation of FE model

Results of the developed FE model were compared with corresponding experimental data in terms of ultimate load (P_u), central deflection accompanying P_u (Δ_c), cracking load (P_{cr}), load-central deflection response (P-Δ) and failure mode. Table 2 shows that P_u, Δ_c, and P_{cr} predicted by the model were all in good agreement with test values, with a maximum divergence of no more than +/-10%. It should be noted that while P_{cr} in the tests was estimated from visual inspections and change in slope of P-Δ curves, it was determined numerically from the tensile damage parameter (d_t) discussed earlier. Fig. 5 plots the
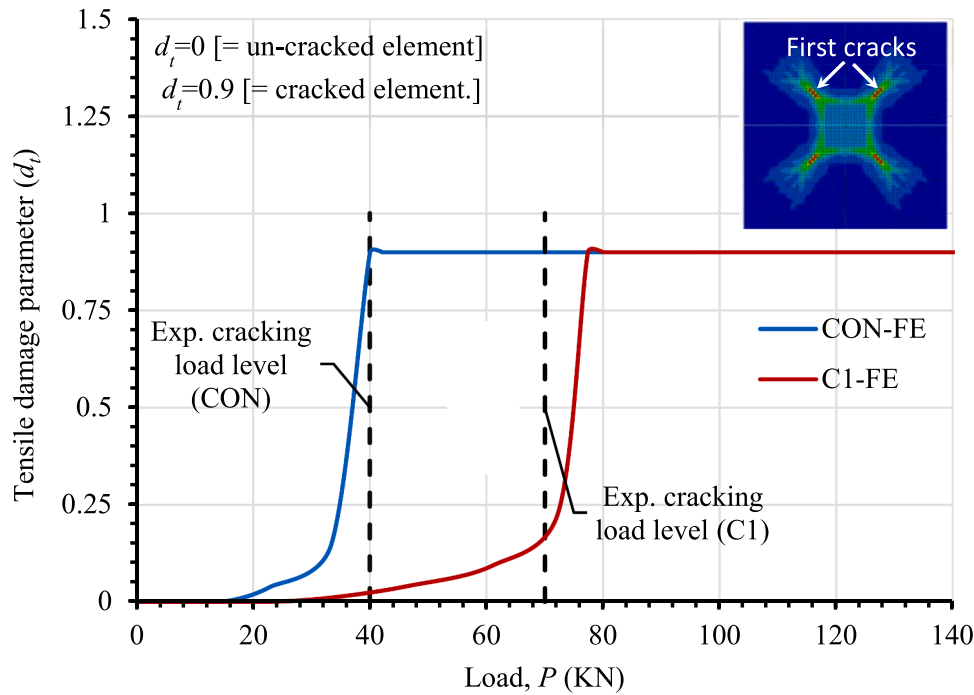
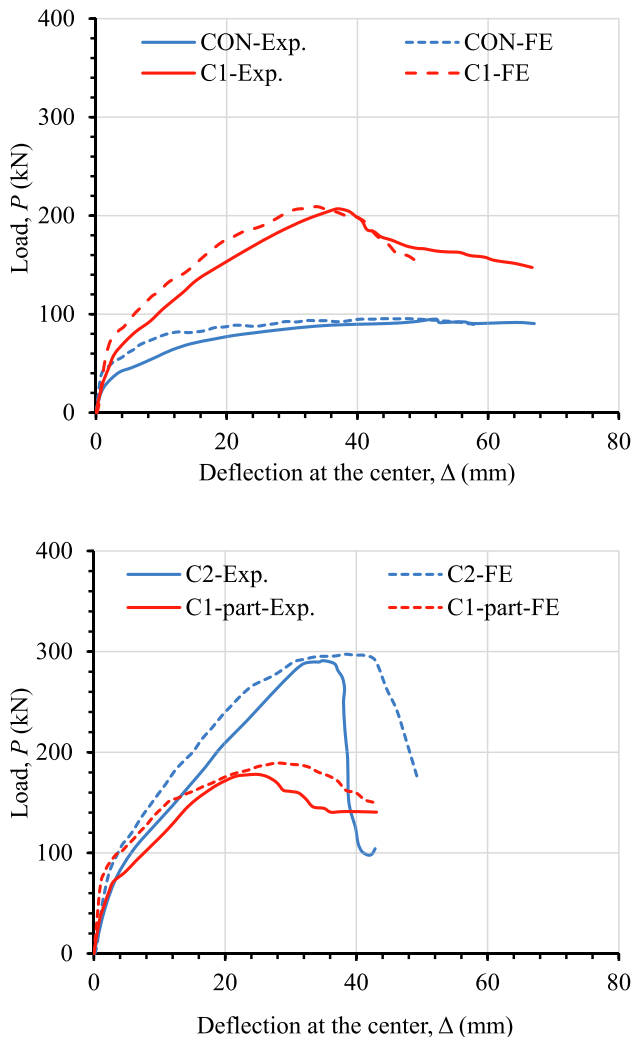**Fig. 5.** Experimental and FE cracking loads for specimens CON and C1.

Fig. 6. Comparison between experimental and FE Load - central deflection curves.

variation of d_t with load (P) for two representative slabs, CON and C1. The parameter was zero (un-cracked) initially, but then increased exponentially and reached a value of 0.9 (cracked) at loads comparable to those estimated experimentally, indicating a good match. Additionally, the first cracks predicted by the model formed diagonally from under loading points toward the slab corners (Fig. 5).

The P-Δ curves from the experiments and FE models are plotted in Fig. 6 for all four slabs. Aside from the slightly stiffer numerical response, which can be due to many reasons including difference in slabs' nominal and actual properties, and model simplifications such as mesh size and material constitutive laws, the model was able to accurately simulate the entire load-deflection response for all slabs. The figure also attests to the model's ability to simulate the effects of FRCM strengthening, including the number of layers and configuration (i.e. half- or full-width).

Another factor to confirm the model's reliability is the ability to capture the observed failure modes. Koutas and Bournas [35] reported two major failure modes, a flexural failure in slabs CON, C1, and C1-part, and a punching shear in slab C2. Additionally, partial slipping of FRCM fibers from the embedding mortar and fiber rupture were also observed in all three strengthened slabs. The flexure failure started by yielding of tensile steel reinforcement, followed by formation of flexural cracks and plastic hinges. The punching shear failure was sudden and brittle, but slab C2 continued to hold some residual strength after P_{max}, due to the development of a membrane resisting mechanism [35]. Fig. 7 depicts the experimentally observed and numerically predicted failure modes in specimen C1 and shows the model's ability to capture the shapes of flexural cracks at the slab's top and bottom faces in addition to simulating the corner uplift phenomenon that typically develops in simply support slabs due to twisting moments. For better visualization and comparison with experimental photos, the "mirror" option available in ABAQUS was used to convert the numerical results from the quarter-size model implemented in this study to those of an equivalent full-size model.

In Fig. 8, the numerically obtained axial stress for an element from a tensile steel rebar located under the loading point, is plotted against the applied load (P), for slabs CON and C1. The figure shows yielding of steel occurred when P increases to 82 kN (or 86% P_u) and 195.9 kN (or 936% P_u) for slabs CON and C1, respectively, confirming with similar

(a) Bottom face cracks.

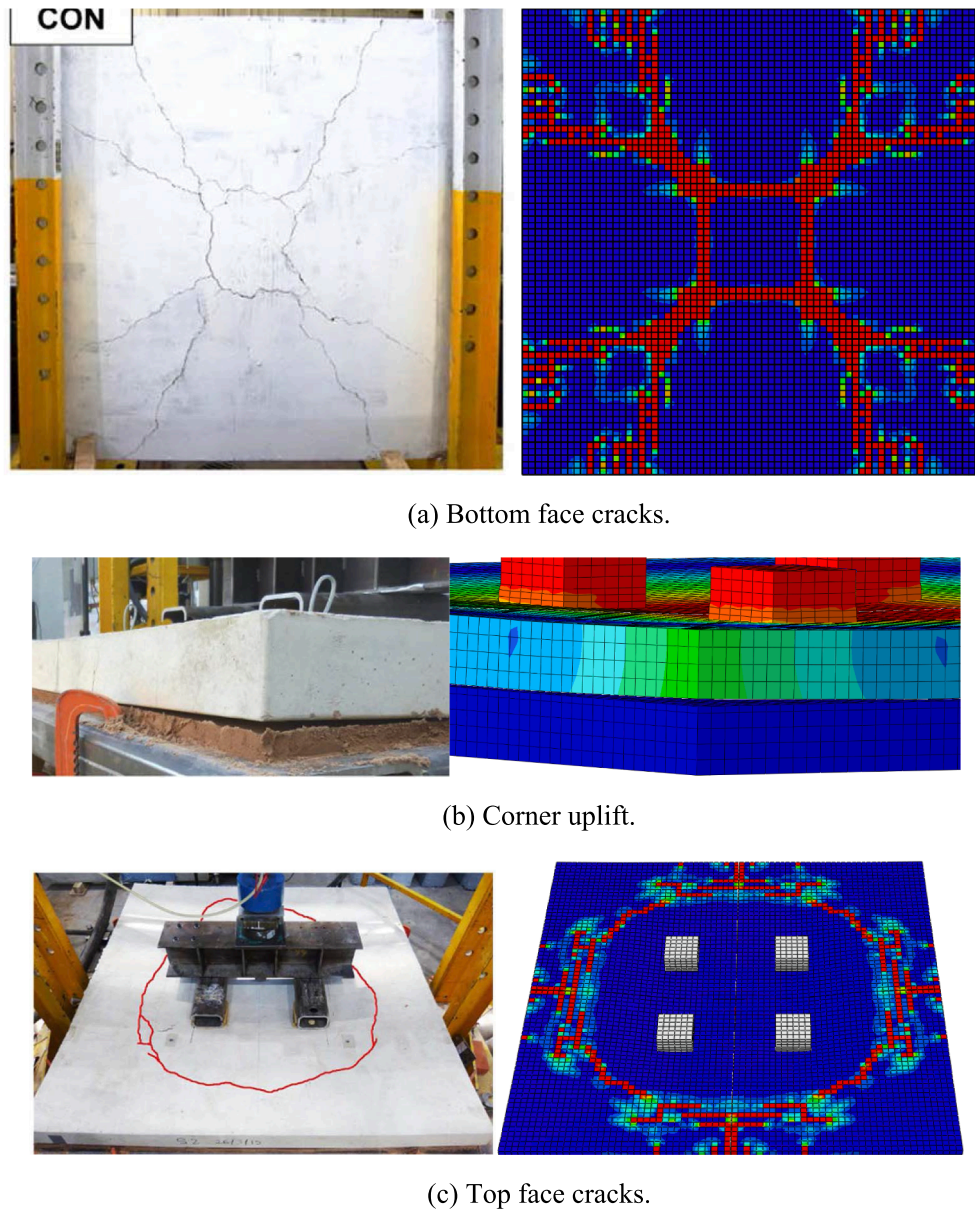(b) Corner uplift.

(c) Top face cracks.

Fig. 7. Crack patterns and corner uplift for slab CON (experimental results are from [35]).

conclusions drawn experimentally from [35]. The difference between the numerical and experimental P at steel yielding are 5 and 10%, for slabs CON and C1, respectively. Furthermore, Fig. 9 shows for slab C1-part the experimentally observed FRCM failures of partial fiber rupture and fiber-mortar slipping, occurring at the cracks that formed at the border of the overlapped orthogonal FRCM layers. The bottom of Fig. 9 shows the numerically obtained damage parameters in fabric (representing fiber rupture) and contact layers (representing slipping). As can be seen, both parameters attained a value of 1.0 (indicative of failure) at the same respective locations in the test where rupture and slipping occurred, confirming the model's ability in capturing these important failure modes.

5. Parametric study

The validated FE model was used to carry out a parametric study into the effects of key variables, namely: FRCM coverage area, use of discontinuous FRCM strips, internal steel reinforcement ratio, concrete compressive strength, and slab aspect ratio. The majority of these parameters are new and have not been evaluated in any of the existing studies on FRCM-strengthened two-way slabs. It should be noted that the basic inputs for the slabs tested by Koutas and Bournas [35] and discussed earlier were maintained in the parametric analysis, except when varying the intended parameter. Forty new models were created in this parametric study. Table 2 lists the properties and key results for a sample of 22 slabs, while the rest are shown graphically.

5.1. FRCM coverage area

The effects of FRCM coverage area was studied preliminarily in [35] using only two cases; slab C1 using one FRCM layer covering the entire tensile face, and slab C1-part (which will be refer here after as C3), using two orthogonal layers each with a width (w_{FRCM}) equals half of the span (S) (Fig. 1). The slab area covered by at least one FRCM layer (A_{FRCM}) in slab C3 is 75% of the total area (A_{slab}). Slab C3 achieved a P_{max} of 87% that of slab C1, with an identical flexural failure mode. In addition to slabs C3 and C1 with a (w_{FRCM}/S) of 0.5 and 1.0, respectively, two additional cases were considered in the parametric study, 0.25 and 0.75
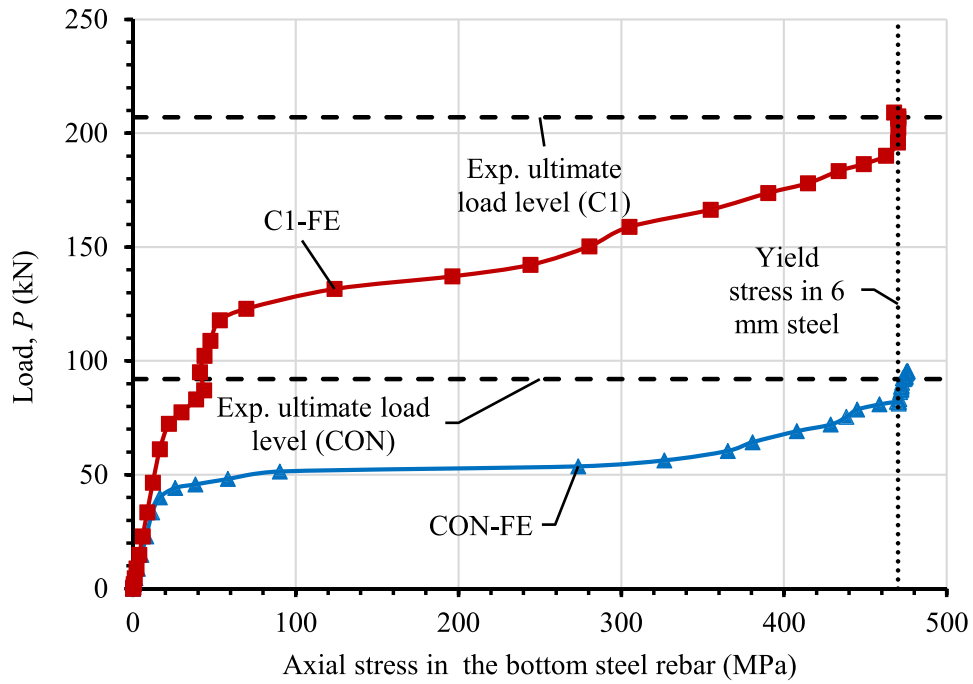
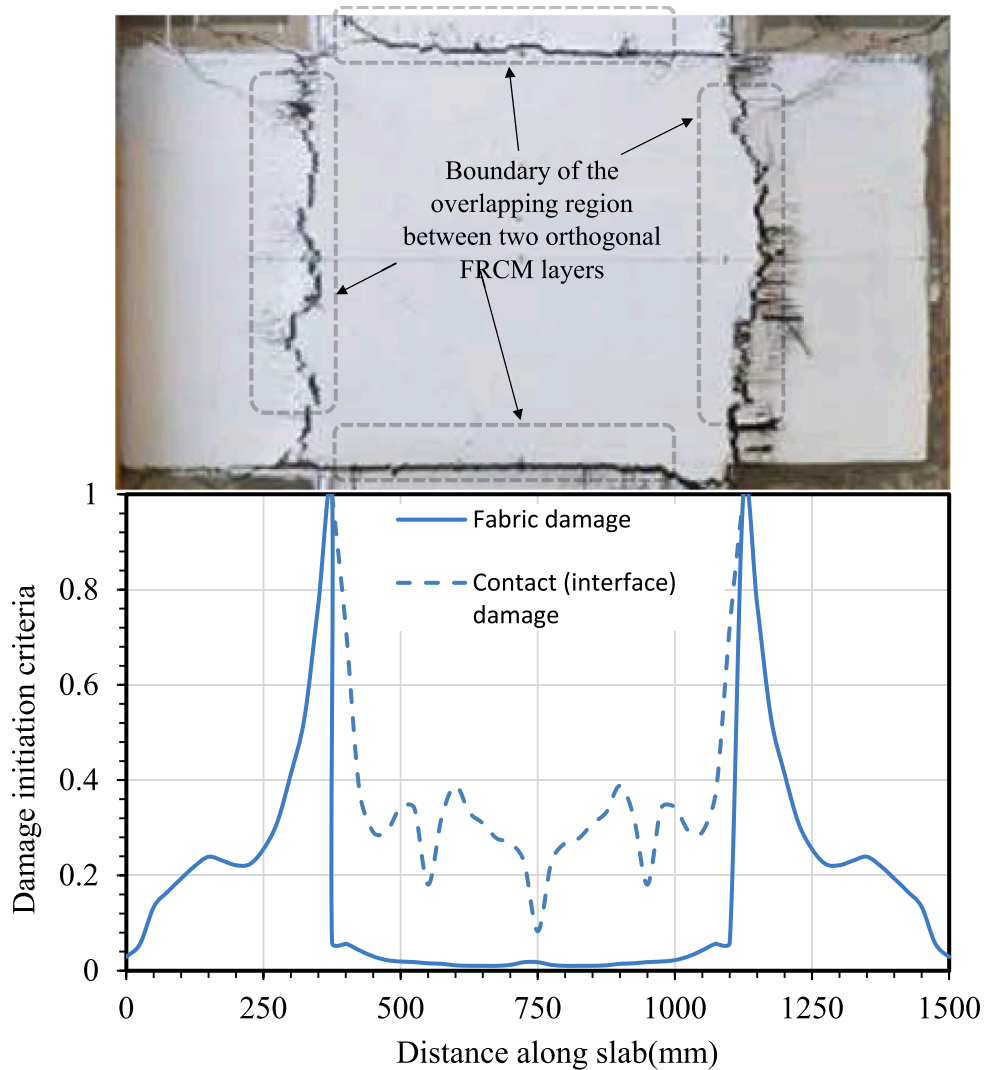**Fig. 8.** Load vs. axial stress in tensile steel reinforcement, showing specimens CON and C1.

Fig. 9. Location of fiber rupture in slab C1-part ((experimental results are from [35]).
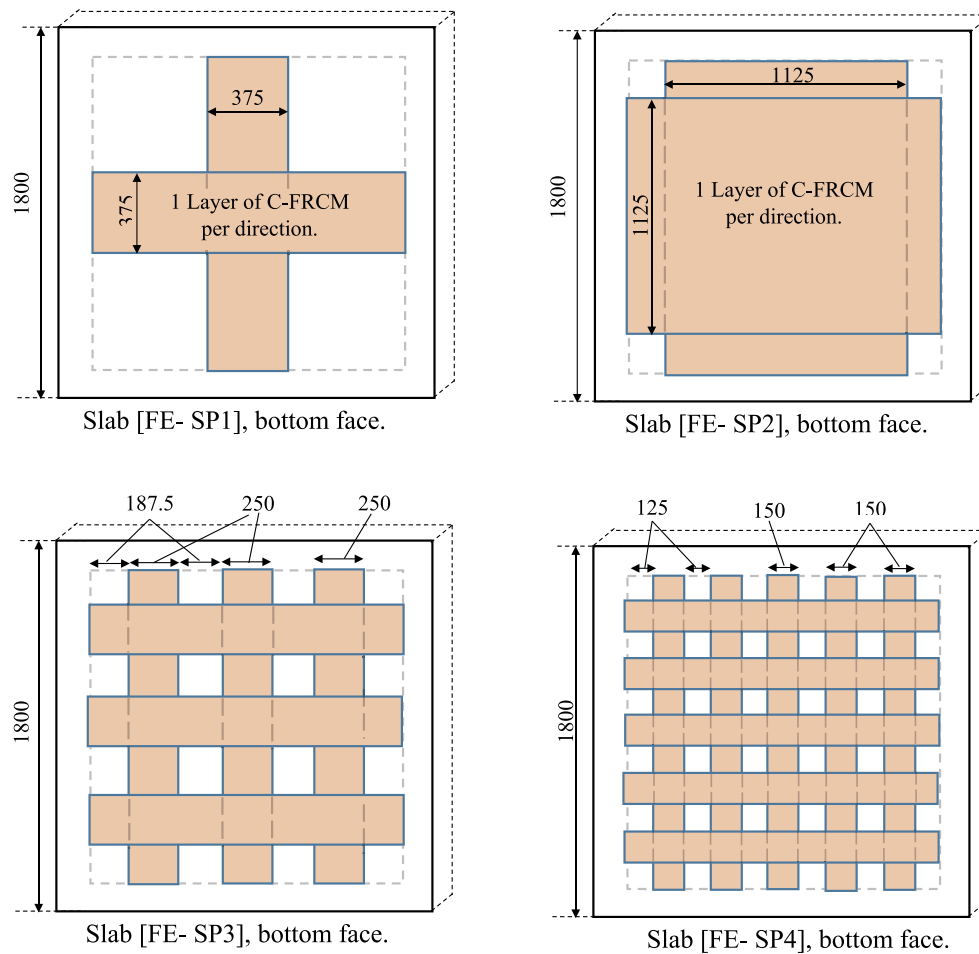
Fig. 10. FRCM reinforcement configuration for slab models in parametric study [note: all dimensions in mm].

(Table. 2), corresponding to respective (A$_{FRCM}$ / A$_{slab}$) of 0.44 and 0.94. The configuration for FRCM reinforcement in the two new slabs is shown in Fig. 10 (top).

Fig. 11(a) shows the *P-Δ* curves for slabs CON (control, w_{FRCM}/S = 0.0), FE-SP1 (w_{FRCM}/S = 0.25), C3 (w_{FRCM}/S = 0.5), FE-SP2 (w_{FRCM}/S = 0.75), and C1 (w_{FRCM}/S = 1.0). In Fig. 11(b), the ultimate load (P_{max}) for each of the five slabs is plotted against (w_{FRCM}/S) ratio. As can be seen from the figures and Table. 2, increasing the FRCM coverage area results in stiffer response, higher ultimate load and more ductility. However, P_u increased sharply by 84% when (w_{FRCM}/S) increased from 0 to 0.25 (or A$_{FRCM}$/ A$_{slab}$ from 0 to 0.44), and then very slightly by 19% when (w_{FRCM}/S) increased from 0.25 to 1 (or A$_{FRCM}$/ A$_{slab}$ from 0.44 to 1). Using a (w_{FRCM}/S) of 0.25 to 0.5 seems to be an efficient and economical option where it results in a comparable 84–90% P_u of that when a full size FRCM layer is used.

5.2. Discontinuous FRCM strips

Slab C3, strengthened by two orthogonal layers, each with a w_{FRCM}/S of 0.5 in each direction was used as a baseline for the comparisons in this section. Two additional models were created, one containing three strips in each direction (slab FE-SP3, Table. 2) and one containing five strips per direction (slab FE-SP4, Table. 2) (Fig. 10 bottom). It should be noted that the total width of discontinuous strips (in each direction) for slabs FE-SP3 and FE-SP4 is equal to that of the one continuous layer in slab C3. The clear distance between strips for slabs FE-SP3 and FE-SP4 were 187.5 and 125 mm respectively.

Fig. 12(a) shows the *P-Δ* curves for slabs with different number of FRCM strips (*N*), namely; CON (*N* = 0), C3 (*N* = 1), FE-SP3 (*N* = 3), and

FE-SP4 (*N* = 5). In Fig. 12(b), (P_{max}) for each of the four slabs is plotted against *N*. Varying the number of strips from 1 to 5 resulted in negligible change in the response and ultimate load. P_{max} decreased by only 3% when *N* is increased from 1 to 5 (Fig. 12(b) and Table. 2). While having minor effects on the structural behavior, the use of discontinuous strips might be preferred in certain applications, such as in slabs with openings or at locations where access to the soffit at some locations is difficult.

5.3. Steel reinforcement ratio

In addition to the slabs in [35] which featured a steel reinforcement ratio (ρ_s) of 0.0017, three values were also investigated, namely: ρ_s = 0.0035, 0.007, 0.013 (Table. 2). The evaluation of ρ_s was performed by changing either the diameter of steel rebars, the spacing between them or both. All four ρ_s values were within the range of minimum (ρ_{min}) and maximum (ρ_{max}) reinforcement ratios, of 0.0022 and 0.0132, respectively. The effects of ρ_s was studied for the slabs, CON (control), C1 (strengthened, w_{FRCM}/S = 1.0), and C3 (strengthened, w_{FRCM}/S = 0.5). All other geometric and material properties were kept constant.

Fig. 13(a, b, c) shows the *P-Δ* curves for the three slabs with ρ_s = 0.0035, 0.007, 0.013, respectively; while Fig. 13(d) plots the relation between (P_{max}) and ρ_s. For strengthened slabs C1 and C3, the variation in P_{max} is almost linear, increasing in average by 77% when ρ_s is increased from 0.0017 to 0.013, however, the contribution of the FRCM system to the total P_{max} appears to be constant starting from ρ_s = 0.0035 and up, whereas at low ρ_s = 0.0017, the contribution of FRCM was significantly higher, indicating a much higher efficiency at lower ρ_s. Fig. 13(a, b, c) shows that while increasing ρ_s from 0.0035 to 0.007 results in an apparent increase of ductility, using a high ρ_s of 0.013 ($\approx \rho_{max}$) leads to a
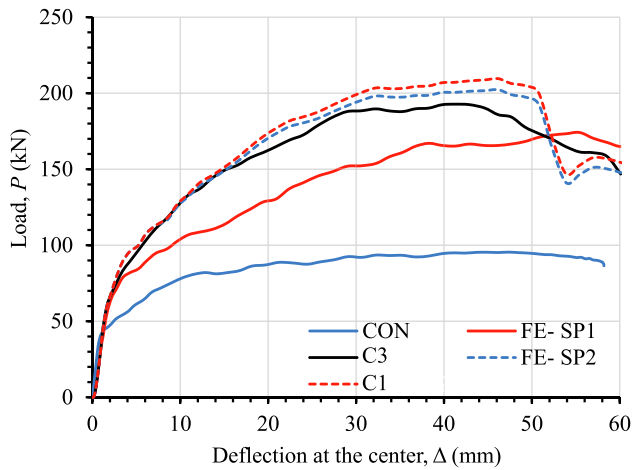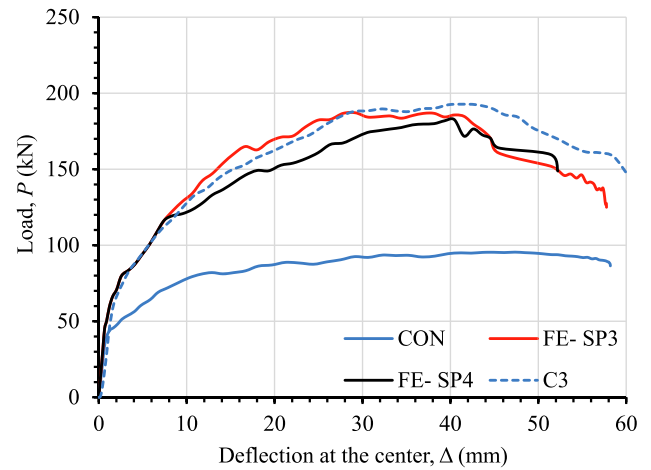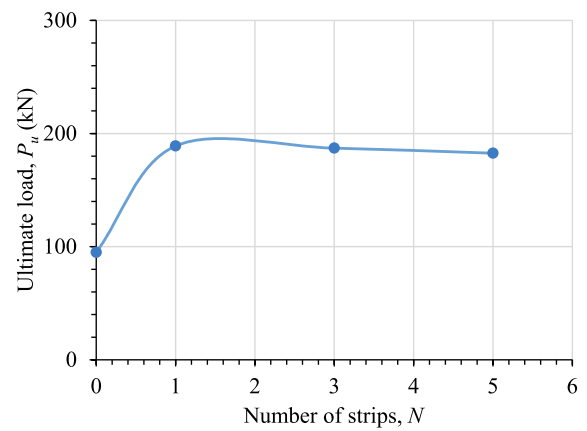
(a) *P*-Δ curves of slabs.
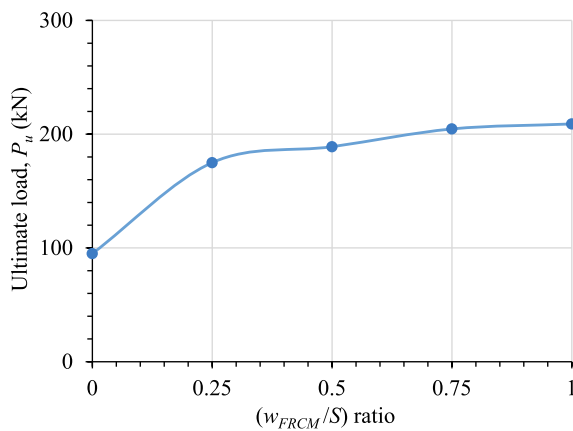
(b) *P*$_u$ vs. (*w*$_{FRCM}$ / *S*) ratio.

Fig. 11. Effects of parameter No. 1 [FRCM coverage area] on behavior of FRCM strengthened two-way RC slabs.

(a) *P*-Δ curves of slabs.

(b) *P*$_u$ vs. number of strips.

Fig. 12. Effects of parameter No. 2 [use of discontinuous FRCM strips] on behavior of FRCM strengthened two-way RC slabs.

decrease in ductility and a steeper post-peak drop in load, indicating a shift of failure mode from flexure to punching shear.

5.4. Concrete compressive strength

In this section, the effects of f_c' are evaluated using three additional values to the 20 MPa tested in [35], namely: 15, 30, and 40 MPa (Table 2). These strengths were studied for three slabs, CON, C1 and C3 and were combined with $\rho_s = 0.0017$ and 0.0035. Higher concrete strengths were not considered in this study as it is less common for slabs or in structures requiring strengthening. Fig. 14(a, b) shows the relation between P_{max} and f_c' for each of the three slabs and the two steel reinforcement ratios. The relation shows an approximately linear trend with the strengthened slabs being more affected by f'_c than the control one. For slabs C1 and C3, P_{max} increased in average by 41% and 33% for $\rho_s = 0.0017$ and 0.0035, respectively, when f'_c is increased from 15 to 40 MPa, whereas for the control slab, P_{max} increased by 27% in average.

5.5. Slab aspect ratio

The slab's aspect ratio, (α) [α = length/width], is an important parameter and is frequently studied for steel-reinforced two way slabs or FRP-strengthened ones [50,51]. However, this parameter has not been evaluated for FRCM-strengthened slabs and existing studies. Three additional values for α are considered in this study, namely: 1.25, 1.5, and 1.75 (Table 2). It should be noted that when constructing the new

models for different aspect ratios, the length for one side of the slab was kept constant and equal to 1800 mm (same as that for slabs in the validation part) while varying the other dimension. In addition, the ratio of FRCM was kept constant in both directions for all aspect ratios and equal to that reported in the experimental campaign.

Fig. 15 shows the relation between P_{max} and α for three slabs, CON, C1 and C3. Except for negligible maximum increase of 4.3% (for slab C1) or maximum decrease of 7.9% (for slab CON), P_{max} does not seem to be affected by the range of aspect ratios considered in this study. However, the concrete cracking pattern was affected by α, as can be seen in Fig. 16 showing the bottom face cracks for slabs CON and C1 at different loads and for α = 1.75. When compared to the cracks in slabs with α = 1.0 (Fig. 7), slabs with α = 1.75 seem to have denser cracks. However, inclined cracks seem to maintain a 45° orientation regardless of aspect ratio.

6. Design equations

In this section the database from the parametric study is used to develop design equations to accurately predict the strength of FRCM strengthened two-way slabs. Two models are available in the literature and are presented next but are also shown to either grossly underestimate or overestimate the strength, in the form of a significant scatter. The models are proposed Koutas and Bournas [38] and ACI 549 [23].

In order to provide simple design equations to predict the bending resistance per unit length of two-way slabs strengthened with FRCM, it is
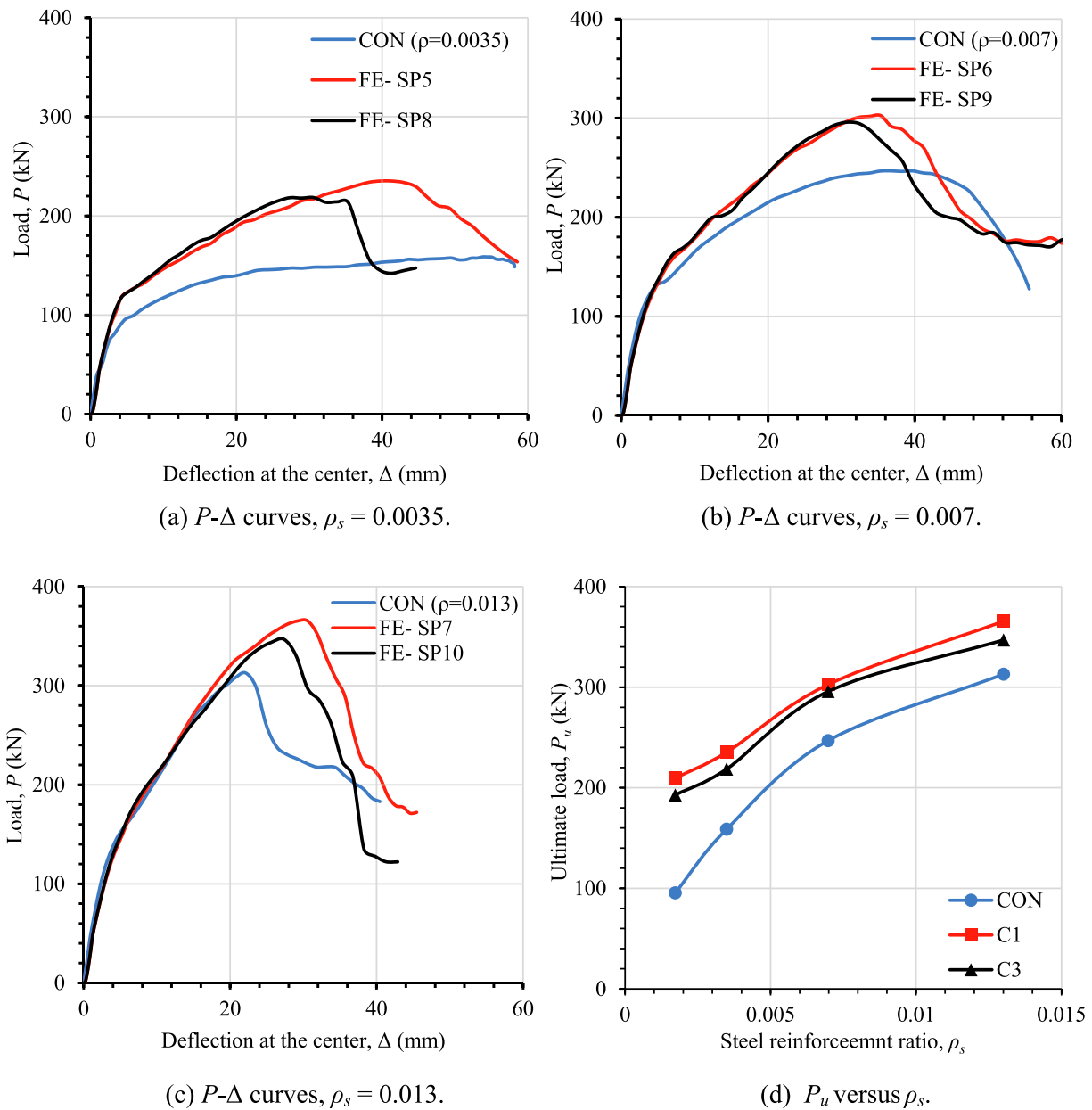
(a) P-Δ curves, $\rho_s = 0.0035$.

(b) P-Δ curves, $\rho_s = 0.007$.

(c) P-Δ curves, $\rho_s = 0.013$.

(d) P_u versus ρ_s.

Fig. 13. Effects of parameter No. 3 [steel reinforcement ratio (ρ_s)] on behavior of FRCM strengthened two-way RC slabs.

important to determine a direct relation between the moment capacity of slabs per unit length (m_r) and the flexural load-bearing capacity (P_u). Equation (5) is used to calculate the moment capacity of the un-strengthened and strengthened slabs, relying on a load to moment calibration factor (k) and P_u:

$$P_u = k \cdot m_r \tag{5}$$

The value of k, determined typically and also in this study from the yield line method, depends on the loading and support conditions, crack pattern, and aspect ratio [52]. For the slabs investigated in this study, k was found to be 15.8, 14.1, 13.5 and 11.4 for aspect ratios of 1, 1.25, 1.50 and 1.75, respectively since the other parameters affecting this value were kept constant in all slabs investigated in this research.

6.1. Koutas and Bournas model

Koutas and Bournas [38] developed an analytical model to predict the bending moment capacity of RC slabs ($m_{r(n)}$) strengthened with

FRCM. The value of $m_{r(n)}$ can be found from Eq. (6), which represents the moment contributions from the internal steel reinforcement (m_s) and the FRCM system (m_f):

$$m_{r(n)} = \rho_s f_y d^2 \left(1 - 0.59 \frac{\rho_s f_y}{f_c'}\right) + F_f \left(h - \frac{x}{2}\right) \tag{6}$$

where ρ_s = steel reinforcement ratio; f_y= yield stress of steel reinforcement; d= slab's effective depth; f_c'= concrete compressive strength; F_f= tensile force in FRCM per unit length; h= slab's total depth, and x = depth of neutral axis.
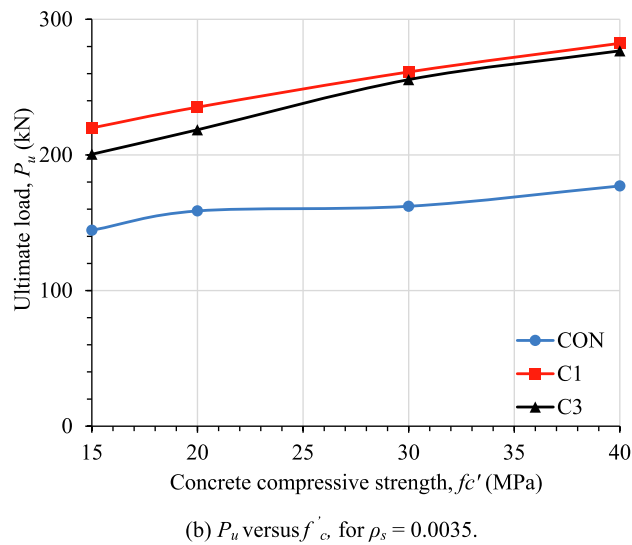
F_f is function of the effective stress in FRCM system (f_{fe}) and can be determined from Eq. (7):

$$F_f = t_f f_{fe} \frac{w_f}{w_s} \tag{7}$$

where t_f and w_f are the thickness and width of FRCM layer and w_s is the slab width. In Koutas and Bournas [38] study, a curve fitting analyses
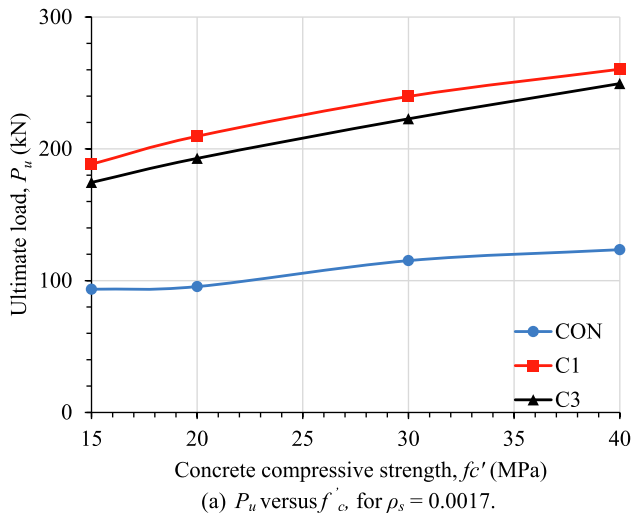
(a) P_u versus f'_c, for $\rho_s = 0.0017$.

(b) P_u versus f'_c, for $\rho_s = 0.0035$.

Fig. 14. Effects of parameter No. 4 [Concrete Compressive Strength (f'_c)] on behavior of FRCM strengthened two-way RC slabs.
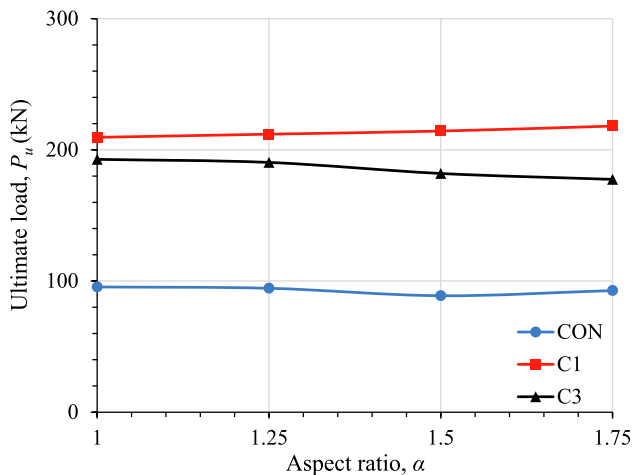

Fig. 15. Effects of parameter No. 5 [slab's aspect ratio (α)] on behavior of FRCM strengthened two-way RC slabsbs.

was used to determine f_{fe}, yielding the following expression as a function of FRCM reinforcement ratio (ρ_f):

$$f_{fe} = 60.2\rho_f^{-0.39} \leq 1200 \text{ MPa} \tag{8}$$

Finally, the depth of neutral axis (x) can be calculated from Eq. (9) bellow, using the concrete strains (ε_c), F_f, and FRCM elastic modulus (E_f):

$$x = h \frac{\varepsilon_c}{\varepsilon_c + F_f/E_f} \tag{9}$$

6.2. ACi-549 [23]

According to ACI-549 [23] code, $m_{r(n)}$ can be determined as:

$$m_{r(n)} = A_s f_s(c_u)\left(d - \frac{\beta_1(c_u)c_u}{2}\right) + \frac{A_f n w_f}{b}f_{fe}(c_u)\left(d_f - \frac{\beta_1(c_u)c_u}{2}\right) \tag{10}$$

where A_s = area of steel reinforcement; $f_s(c_u)$ = steel's tensile stress at failure and can be determined from Eq. (11); $\beta_1(c_u)$ = concrete stress block factor; c_u = depth of neutral axis; n = number of FRCM plies; $f_{fe}(c_u)$, d_f, and A_f = effective tensile stress, effective depth, and cross-sectional area for FRCM reinforcement, respectively; w_f and b = width of FRCM reinforcement and slab, respectfully.

$$f_s(c_u) = \begin{vmatrix} \varepsilon_s(c_u) \cdot E_s \text{ if}(\varepsilon_s(c_u) \cdot E_s) \leq f_y \\ f_y \text{ otherwise} \end{vmatrix} \tag{11}$$

where $\varepsilon_s(c_u)$ = steel tensile strain at failure which can be calculated from Eq. (12), and E_s = modulus of elasticity for steel reinforcement.

$$\varepsilon_s(c_u) = (\varepsilon_{fe} + \varepsilon_{bi}) \cdot \left(\frac{d - c_u}{h - c_u}\right) \tag{12}$$

where ε_{fe} = effective tensile strain in FRCM reinforcement, determined as the minimum of design tensile strain (ε_{fd}) and a strain of 0.012; ε_{bi} = existing tensile strain at slab's bottom in case loading is present prior to strengthening [$\varepsilon_{bi} = 0$ in this study]; and h = depth of slab. $\beta_1(c_u)$ can be found from Eq. (13):

$$\beta_1(c_u) = \frac{4\varepsilon_c' - \varepsilon_c(c_u)}{6\varepsilon_c' - 2\varepsilon_c(c_u)} \tag{13}$$

where ε_c' = concrete's compressive strain at f_c' and can be found from Eq. (14) according to ACI-318 [43]; and $\varepsilon_c(c_u)$ = concrete's compressive strain at failure, determined from Eq. (15):

$$\varepsilon_c' = \frac{1.7f_c'}{E_c} \tag{14}$$

$$\varepsilon_c(c_u) = (\varepsilon_{fe} + \varepsilon_{bi}) \cdot \left(\frac{c_u}{h - c_u}\right) \tag{15}$$

The solution procedure starts by assuming a recommended initial value, $c_{u1} = 0.2 d$, for the neutral axis depth (c_u); then force equilibrium is checked using Eq. (16) which calculates a new value for c_u, c_{u2}. If the difference between c_{u1} and c_{u2} is over 5%, a new value is given to c_{u1} and the iterative process is repeated until equilibrium is satisfied and difference is less than 5%.

$$c_{u2} = \frac{A_s b f_s(c_{u1}) + A_f n w_f f_{fe}(c_{u1})}{\alpha_1(c_{u1})f_c'\beta_1(c_{u1})b} \tag{16}$$

Finally, the effective tensile stress in FRCM reinforcement $f_{fe}(c_u)$ is computed from Eq. (17), which is dependent on the FRCM's elastic modulus (E_f) and its effective tensile strain ($\varepsilon_{fe1}(c_u)$) as determined from
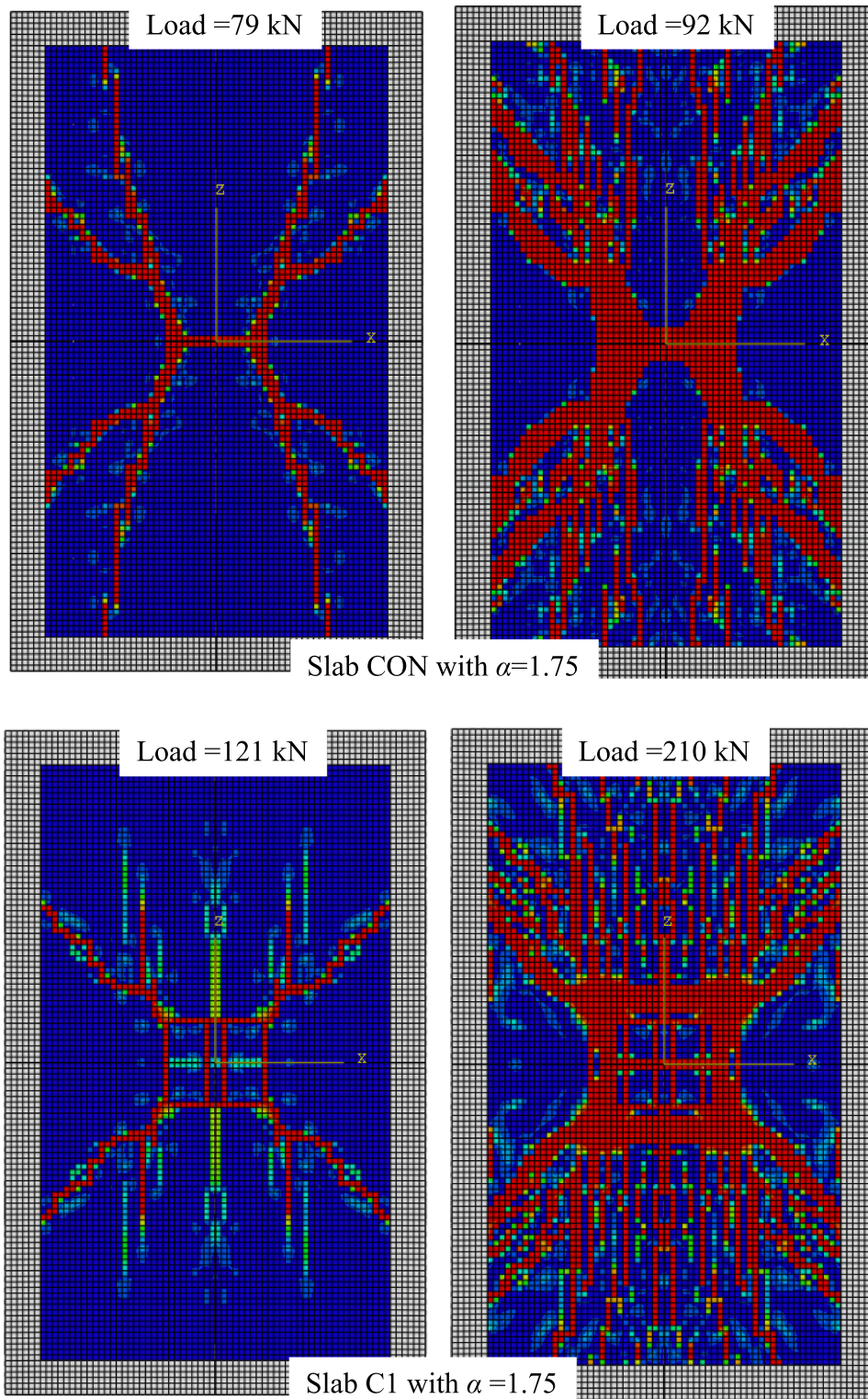
Fig. 16. Crack patterns at different loads, for slabs with aspect ratio (α) of 1.75.

Eq. (18):

$$f_{fe}(c_u) = E_f \cdot \varepsilon_{fe1}(c_u) \tag{17}$$

$$\varepsilon_{fe1}(c_u) = \left| \begin{array}{l} \left[0.003 \left(\dfrac{h - c_u}{c_u} \right) - \varepsilon_{bi} \right] if \, 0.003 \left(\dfrac{h - c_u}{c_u} \right) - \varepsilon_{bi} \leq \varepsilon_{fe} \\ \qquad\qquad \varepsilon_{fe} \, otherwise \end{array} \right. \tag{18}$$

6.3. Proposed model

A regression analysis was performed on the database from the parametric study to develop an accurate expression for the FRCM effective strain (ε_{fe}). Equation (19) presents the final formula, obtained with an R^2 of 0.90, showing that ε_{fe} is depenednet on four variables, namely: steel reinforcement ratio (ρ_s), FRCM reinforcement ratio (ρ_f), concrete compressive strength (f_c'), and the slab's aspect ratio (α).
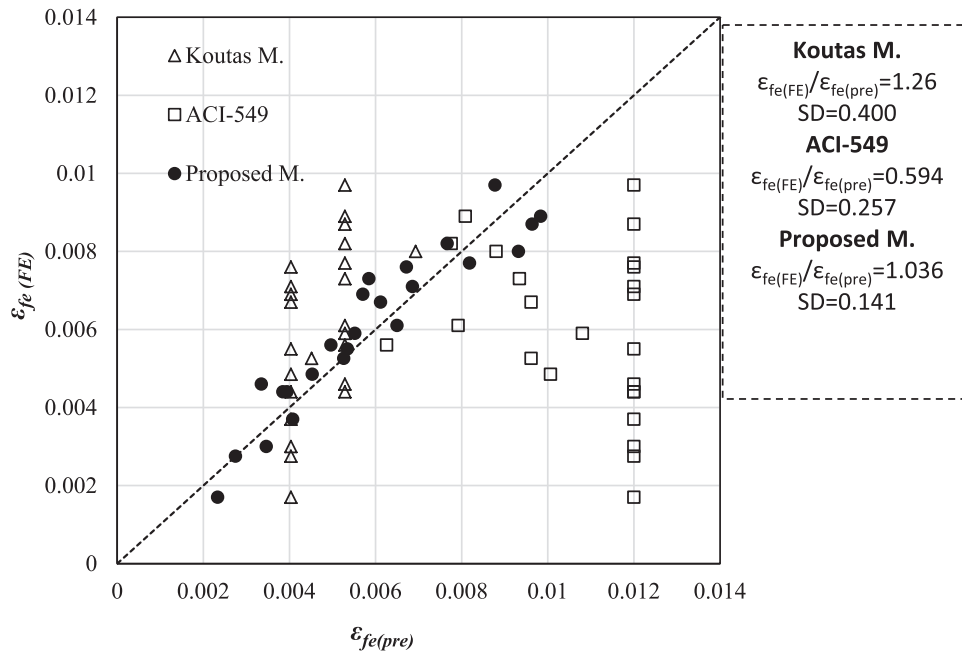
Fig. 17. FE-based vs. analytically-predicted FRCM's effective strains, comparing predictions from Koutas model, ACI-549 model, and proposed mod.

$$\varepsilon_{fe} = 2.45 \times 10^{-7} \rho_f^{-0.52} \rho_s^{-0.71} f_c'^{-0.56} \alpha^{0.74} \qquad (19)$$

Equation (20), also determined from regression analysis, presents a further simplified version of Eq. (19), intended for practical design applications.

$$\varepsilon_{fe} = 1.3 \times 10^{-6} \sqrt{\frac{f_c' \alpha}{\rho_f \rho_s}} \qquad (20)$$

6.4. Evaluation of the existing models

The effective strain in FRCM reinforcement (ε_{fe}) can be used to assess the accuracy of the two existing analytical models. Fig. 17 plots the relation between the FE-based ε_{fe} ($\varepsilon_{fe\,(FE)}$) and that predicted by the analytical models ($\varepsilon_{fe\,(pre)}$) using Eq. (19). It can be seen from this figure that ACI-549 model provided relatively unrealistic predictions where its mean value for ($\varepsilon_{fe(FE)}/\varepsilon_{fe(pre)}$) was 0.594 and its standard deviation (SD) was 0.257. The model by Koutas and Bournas [38], referred to hereafter as Koutas M for simplicity, resulted in a mean value for ($\varepsilon_{fe(FE)}/\varepsilon_{fe(pre)}$) of 1.26, and a SD of 0.400. Although this model presented a reasonable estimate for the effective strain, its standard deviation was significantly high, reflecting a significant scatter in predictions.

Fig. 18(a, b, c) plot the relation between the FE-based and analytically-predicted (ε_{fe}) versus three parameters that were studied in the parametric study, namely: concrete compressive strength (f_c'), FRCM reinforcement ratio (ρ_f), and aspect ratio (α), on the effective strain (ε_{fe}), respectively. As demonstrated earlier, ε_{fe} typically increases with f_c' and α, but decreases with ρ_f. It should be noted that ε_{fe} were measured in the FRCM layer in the shorter direction for slabs with aspect ratio > 1.0. Although the ACI-549 model showed a similar trend at some points, its predictions of ε_{fe} in most cases differed significantly from the FE values, with a maximum divergence of 3 times $\varepsilon_{fe\,(FE)}$. On the other hand, the model by Koutas and Bournas [38] was not able to capture the relation between ε_{fe} and f_c' and α, because the model was derived from limited experimental data set that did not vary these two variables. In contrast, and because the experiments included several ρ_f ratios, the model correctly captured the ε_{fe} behavior in relation to FRCM reinforcement ratio (Fig. 18(b)).

Fig. 19 plots the relation between FE-based and analytically

predicted ultimate loads (P_u) of FRCM-strengthened slabs. It can be seen from this figure that the ACI-549 model results in unsafe (over predictions) of P_u compared to the FE results. The Koutas M yielded better P_u estimations but showed a significant scatter (SD = 0.212). The above results show that further effort is still needed to refine existing analytical predictions and develop a model capable of accurately predicting the response of FRCM-strengthened two-way RC slabs.

Predictions of Eq. (19) for ε_{fe} are plotted in Figs. 17 and 18, in comparisons with results from the FE simulations and the two existing analytical models. The proposed model was able to accurately predict ε_{fe}, with a mean value of ($\varepsilon_{fe(FE)}/\varepsilon_{fe(pre)}$) and a SD of 1.036 and 0.141, respectively, for the original form in Eq. (19), and 0.998 and 0.153, for the simplified version in Eq. (20). In addition, ε_{fe} from the proposed model agreed with the FE model results and was able to capture the variation of ε_{fe} with f_c, ρ_f, and α (Fig. 18).

The ε_{fe} from the proposed model were used in conjunction with the analytical procedure outlined in Koutas and Bournas [35] study to determine the ultimate load (P_u) and moment resistance $m_{r(n)}$. Fig. 19 shows the P_u predictions from the analytical procedure using the proposed model for ε_{fe}, along with those from FE simulation and other existing analytical models. P_u values from the proposed model were in much better agreement with FE data than those from the existing analytical models, with a mean value of $P_{u(FE)}/P_{u(pre)}$ of 1.06 and a SD of 0.065.

7. Conclusions and recommnedations

Fabric reinforced cementitious mortar (FRCM) has become a viable technique to strengthen, repair, and confine concrete elements, and a sustainable alternative to conventional epoxy-bonded fiber reinforced polymer (FRP) systems. While the technique is amply studied and applied on beams and columns, its utilization for two-way RC slabs has rather been very limited. Based on the results of a robust finite element model developed for FRCM-strengthened slabs and a comprehensive parametric study performed on several material and geometric variables, the following conclusions can be drawn:

- Comparing with a recent experimental study, the FE model predictions agreed very well with test data in terms of load-deflection
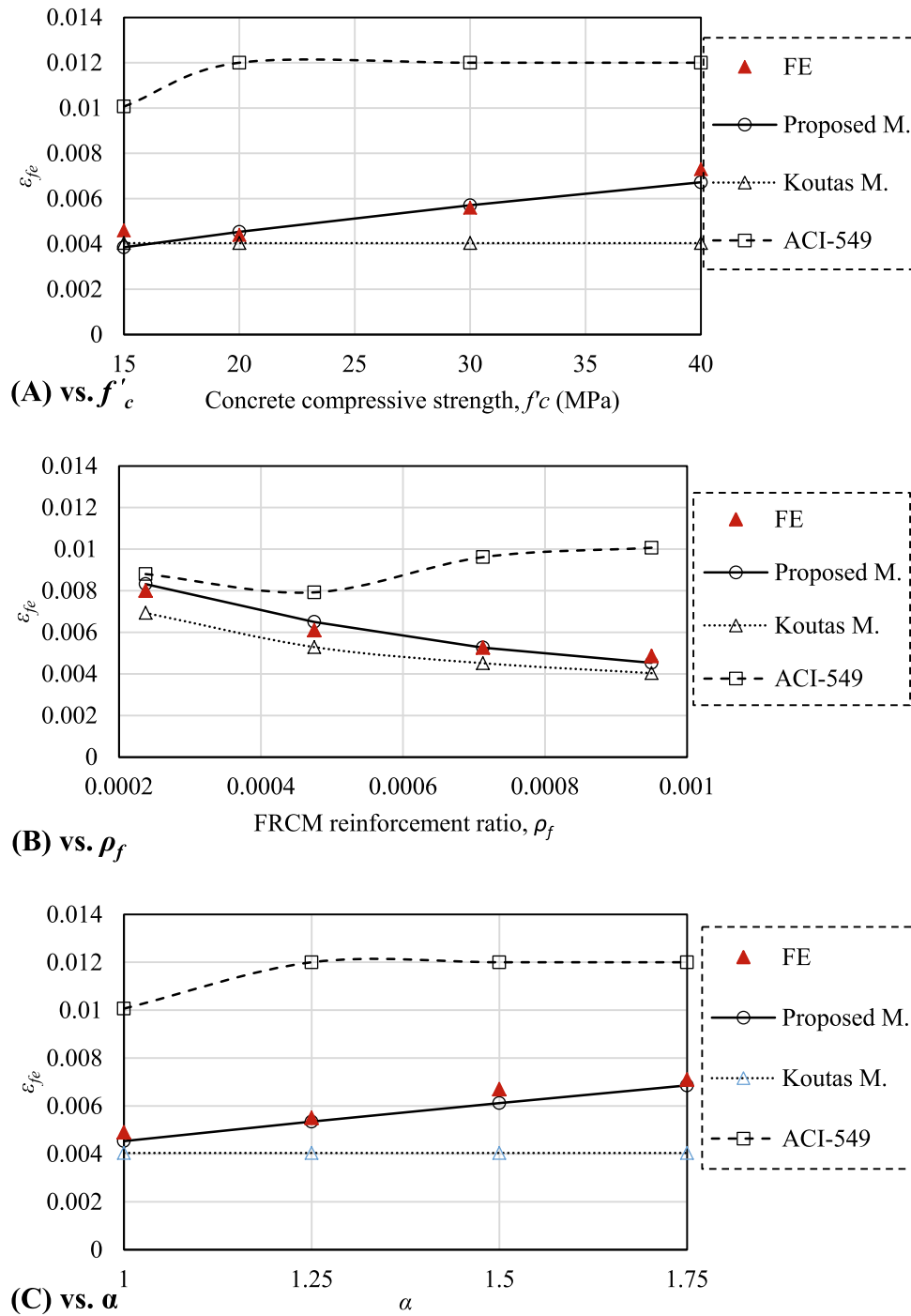
(A) vs. f'_c

(B) vs. ρ_f

(C) vs. α

Fig. 18. FRCM's effective strain (ε_{fe}) vs. f_c', ρ_f, and α, from FE simulations and analytical models..

curves, failure modes, and general behavior, with a maximum divergence of ±10% for ultimate loads (P_u), and deflection at P_u.

- Increasing the width of FRCM reinforcement (w_{FRCM})-to-span (S) ratio [w_{FRCM}/S] from 0 to 0.25 results in a sharp increase in P_u, by 84%. Further increase in [w_{FRCM}/S] ratio from 0.25 to 1.0, results in only a small gain of 19% increase in P_u. Therefore, using [w_{FRCM}/S] ratio of 0.25–0.5 is recommended.
- The use of multiple discontinuous FRCM strips in lieu of one continuous strip has an insignificant effect on P_u. It may be useful, however, when the slab soffit is not entirely accessible for strengthening.
- Varying the internal steel reinforcement ratio (ρ_s) from 0.0035 to 0.013 resulted in 77% increase in P_u for the FRCM-strengthened

slabs. The contribution of FRCM to P_u, however, over the range of (ρ_s) is constant. At a high ρ_s of 0.013 ductility is reduced and a shift in failure mode from flexure to punching shear occurs.

- For strengthened slabs with [w_{FRCM}/S] = 0.5 and 1.0, P_u increased by 41 and 33%, respectively, when the concrete compressive strength (f_c') is varied from 20 to 40 MPa. For the same respective range of f_c', P_u of control slab increased by 27%.
- Varying the slab aspect ratio from 1 to 1.75 resulted in a negligible change in P_u for both the control and strengthened slabs.
- Predictions of P_u and FRCM effective strain (ε_{fe}) from two existing analytical models were found to be mostly unconservative, highly scattered or insensitive to several geometric and material properties.
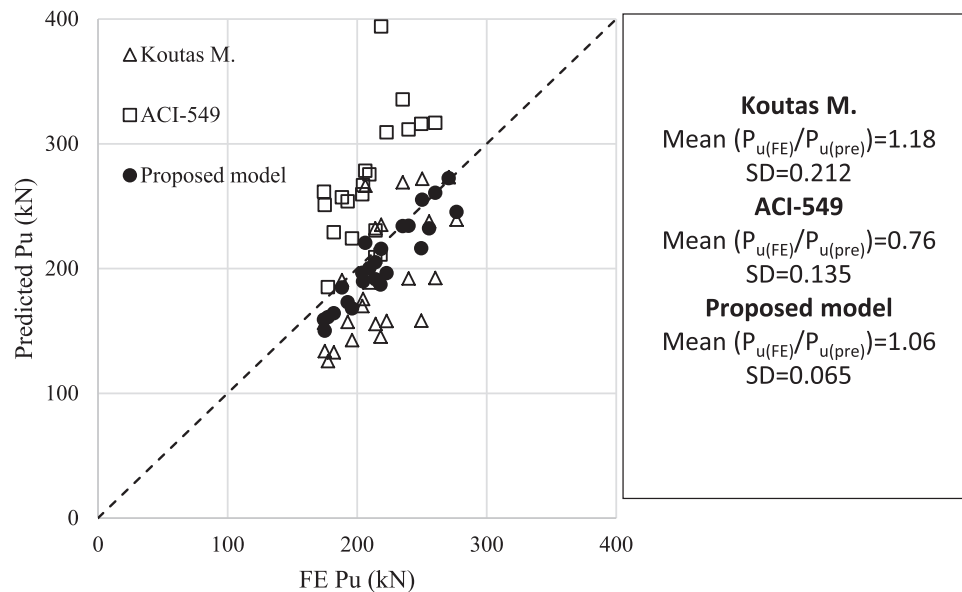
Fig. 19. FE-based vs. analytically-predicted ultimate load (P_u), comparing predictions from Koutas model, ACI-549 model, and proposed model.

- A new analytical model was developed and presented for ε_{fe}, based on regression analysis of data from the numerical parametric study. It outperformed the existing analytical models and resulted in P_u values at excellent agreement with numerical results and a very small standard deviation.

Given the scarcity of research on the studied topic and lack of large experimental data to draw solid conclusions in addition to the numerical nature of the current article and associated approximations, e.g. material idealizations, and effects of mesh size, etc., the results and developed design models should be used with caution, optimally within the range of material and geometric properties considered in this research. Further experimental tests are certainly warranted to expand the result database, test, and refine the presented design equations.

CRediT authorship contribution statement

Majid M.A. Kadhim: Conceptualization, Methodology, Investigation, Validation, Writing – original draft, Writing – review & editing, Formal analysis. **Akram Jawdhari:** Conceptualization, Methodology, Writing – original draft, Writing – review & editing, Visualization, Formal analysis. **Ali Hadi Adheem:** Formal analysis, Investigation, Writing – original draft. **Amir Fam:** Writing – review & editing, Visualization, Resources.

Declaration of Competing Interest

The authors declare that they have no known competing financial interests or personal relationships that could have appeared to influence the work reported in this paper.

References

[1] Täljsten B, Blanksvärd T. Mineral-based bonding of carbon FRP to strengthen concrete structures. J Compos Constr 2007;11(2):120–8.

[2] ACI. Guide for the design and construction of structural concrete reinforced with fiber-reinforced polymer (FRP) bars. ACI 440 Farmington Hills, MI: ACI (American Concrete Institute); 2015.

[3] Al-Bayati G, Al-Mahaidi R, Kalfat R. Experimental investigation into the use of NSM FRP to increase the torsional resistance of RC beams using epoxy resins and cement-based adhesives. Constr Build Mater 2016;124:1153–64.

[4] Jawdhari A, Harik I. Finite element analysis of RC beams strengthened in flexure with CFRP rod panels. Constr Build Mater 2018;163:751–66.

[5] Abouzied A, Masmoudi R. Structural performance of new fully and partially concrete-filled rectangular FRP-tube beams. Constr Build Mater 2015;101:652–60.

[6] Kadhim MMA, Jawdhari AR, Altaee MJ, Adheem AH. Finite element modelling and parametric analysis of FRP strengthened RC beams under impact load. J Build Eng 2020;32:101526. https://doi.org/10.1016/j.jobe.2020.101526.

[7] Ren W, Sneed LH, Gai Y, Kang X. Test results and nonlinear analysis of RC T-beams strengthened by bonded steel plates. Int J Concr Struct Mater 2015;9(2):133–43.

[8] Mostofinejad D, Shameli SM. Externally bonded reinforcement in grooves (EBRIG) technique to postpone debonding of FRP sheets in strengthened concrete beams. Constr Build Mater 2013;38:751–8.

[9] Al-Mahmoud F, Castel A, Minh TQ, François R. Reinforced concrete beams strengthened with NSM CFRP rods in shear. Adv Struct Eng 2015;18(10):1563–74.

[10] Capozucca R. On the strengthening of RC beams with near surface mounted GFRP rods. Compos Struct 2014;117:143–55.

[11] Kadhim MMA, Adheem AH, Jawdhari AR. Nonlinear finite element modelling and parametric analysis of shear strengthening RC T-beams with NSM CFRP technique. Int J Civ Eng 2019;17(8):1295–306.

[12] Jawdhari A, Harik I, Fam A. Behavior of reinforced concrete beams strengthened with CFRP rod panels CRP 195. Structures 2018;16:239–53.

[13] Jawdhari A, Peiris A, Harik I. Experimental study on RC beams strengthened with CFRP rod panels. Eng Struct 2018;173:693–705.

[14] Jawdhari A, Semendary A, Fam A, Khoury I, Steinberg E. Bond Characteristics of CFRP Rod Panels Adhered to Concrete under Bending Effects. J Compos Constr 2019;23(1):04018077. https://doi.org/10.1061/(ASCE)CC.1943-5614.0000909.

[15] Zhao X-L, Zhang L. State-of-the-art review on FRP strengthened steel structures. Eng Struct 2007;29(8):1808–23.

[16] Peiris A, Harik I. Steel bridge girder strengthening using postinstalled shear connectors and UHM CFRP laminates. J Perform Constr Facil 2015;29(5):04014139. https://doi.org/10.1061/(ASCE)CF.1943-5509.0000625.

[17] Al-Jaberi Z, Myers JJ, ElGawady MA. Experimental and analytical approach for prediction of out-of-plane capacity of reinforced masonry walls strengthened with externally bonded FRP laminate. J Compos Constr 2019;23(4):04019026. https://doi.org/10.1061/(ASCE)CC.1943-5614.0000947.

[18] Al-Jaberi Z, Myers JJ, ElGawady MA. Out-of-Plane Flexural Behavior of Reinforced Masonry Walls Strengthened with Near-Surface-Mounted Fiber-Reinforced Polymer. ACI Struct J 2018;115.

[19] Raoof SM, Bournas DA. Bond between TRM versus FRP composites and concrete at high temperatures. Compos B Eng 2017;127:150–65.

[20] Aljazaeri ZR, Myers JJ. Flexure performance of RC one-way slabs strengthened with composite materials. J Mater Civ Eng 2018;30(7):04018120. https://doi.org/10.1061/(ASCE)MT.1943-5533.0002299.

[21] Bencardino F, Carloni C, Condello A, Focacci F, Napoli A, Realfonzo R. Flexural behaviour of RC members strengthened with FRCM: State-of-the-art and predictive formulas. Compos B Eng 2018;148:132–48.

[22] Jawdhari A, Fam A, Harik I. Bond between CFRP rod panels and concrete using cementitious mortar. Constr Build Mater 2020;235:117503. https://doi.org/10.1016/j.conbuildmat.2019.117503.

[23] ACI. Guide to design and construction of externally bonded Fabric-Reinforced Cementitious Matrix (FRCM) systems for repair and strengthening concrete and masonry structures. ACI 549.4 R, American Concrete Institute Farmington Hills, MI; 2013.

[24] Sneed LH, Verre S, Carloni C, Ombres L. Flexural behavior of RC beams strengthened with steel-FRCM composite. Eng Struct 2016;127:686–99.

[25] Koutas LN, Tetta Z, Bournas DA, Triantafillou TC. Strengthening of concrete structures with textile reinforced mortars: state-of-the-art review. Am Soc Civ Eng 2019;23(1):03118001. https://doi.org/10.1061/(ASCE)CC.1943-5614.0000882.

[26] Tetta ZC, Bournas DA. TRM vs FRP jacketing in shear strengthening of concrete members subjected to high temperatures. Compos B Eng 2016;106:190–205.

[27] Alabdulhady MY, Sneed LH, Carloni C. Torsional behavior of RC beams strengthened with PBO-FRCM composite–an experimental study. Eng Struct 2017; 136:393–405.

[28] Jawdhari A, Adheem AH, Kadhim MMA. Parametric 3D finite element analysis of FRCM-confined RC columns under eccentric loading. Eng Struct 2020;212:110504. https://doi.org/10.1016/j.engstruct.2020.110504.

[29] Ombres L. Flexural analysis of reinforced concrete beams strengthened with a cement based high strength composite material. Compos Struct 2011;94(1): 143–55.

[30] Bournas DA, Lontou PV, Papanicolaou CG, Triantafillou TC. Textile-reinforced mortar versus fiber-reinforced polymer confinement in reinforced concrete columns. ACI Struct J 2007;104:740.

[31] Triantafillou TC, Papanicolaou CG, Zissimopoulos P, Laourdekis T. Concrete confinement with textile-reinforced mortar jackets. ACI Mater J 2006;103:28.

[32] Meriggi P, de Felice G, De Santis S. Design of the out-of-plane strengthening of masonry walls with Fabric Reinforced Cementitious Matrix composites. Constr Build Mater 2020;240:117946. https://doi.org/10.1016/j.conbuildmat.2019.117946.

[33] De Santis S, De Canio G, de Felice G, Meriggi P, Roselli I. Out-of-plane seismic retrofitting of masonry walls with Textile Reinforced Mortar composites. Bull Earthq Eng 2019;17(11):6265–300.

[34] Koutas LN, Bournas DA. Out-of-plane strengthening of masonry-infilled RC frames with textile-reinforced Mortar Jackets. J Compos Constr 2019;23(1):04018079. https://doi.org/10.1061/(ASCE)CC.1943-5614.0000911.

[35] Koutas LN, Bournas DA. Flexural strengthening of two-way RC slabs with textile-reinforced mortar: experimental investigation and design equations. J Compos Constr 2017;21(1):04016065. https://doi.org/10.1061/(ASCE)CC.1943-5614.0000713.

[36] Loreto G, Leardini L, Arboleda D, Nanni A. Performance of RC slab-type elements strengthened with fabric-reinforced cementitious-matrix composites. J Compos Constr 2014;18:A4013003.

[37] Papanicolaou C, Triantafillou T, Papantoniou I, Balioukos C. Strengthening of two-way reinforced concrete slabs with textile reinforced mortars (TRM); 2009.

[38] Koutas LN, Bournas DA. Flexural Strengthening of Two-Way RC Slabs with Cut Openings Using Textile-Reinforced Mortar Composites. J Compos Constr 2021;25: 04021018.

[39] Simulia DS. Abaqus 2016 analysis user's manual. Providence, RI: Simulia; 2016.

[40] Kadhim MMA, Wu Z, Cunningham LS. Numerical study of full-scale CFRP strengthened open-section steel columns under transverse impact. Thin-Walled Struct 2019;140:99–113.

[41] Altaee M, Cunningham LS, Gillie M. Practical application of CFRP strengthening to steel floor beams with web openings: a numerical investigation. J Constr Steel Res 2019;155:395–408.

[42] Nguyen HT, Kim SE. Finite element modeling of push-out tests for large stud shear connectors. J Constr Steel Res 2009;65(10-11):1909–20.

[43] ACI. Building Code Requirements for Structural Concrete (ACI 318-14) and Commentary on Building Code Requirements for Structural Concrete. American Concrete Institute Farmington Hills, MI; 2014.

[44] Genikomsou AS, Polak MA. Finite element analysis of punching shear of concrete slabs using damaged plasticity model in ABAQUS. Eng Struct 2015;98:38–48.

[45] Kent DC, Park R. Flexural members with confined concrete. J Struct Div 1971;97 (7):1969–90.

[46] Younis A, Ebead U. Bond characteristics of different FRCM systems. Constr Build Mater 2018;175:610–20.

[47] Zou X, Sneed LH, D'Antino T, Carloni C. Analytical Bond-Slip Model for Fiber-Reinforced Cementitious Matrix-Concrete Joints Based on Strain Measurements. J Mater Civ Eng 2019;31(11):04019247. https://doi.org/10.1061/(ASCE) MT.1943-5533.0002855.

[48] D'Antino T, Sneed LH, Carloni C, Pellegrino C. Influence of the substrate characteristics on the bond behavior of PBO FRCM-concrete joints. Constr Build Mater 2015;101:838–50.

[49] Carloni C, D'Antino T, Sneed LH, Pellegrino C. Role of the matrix layers in the stress-transfer mechanism of FRCM composites bonded to a concrete substrate. J Eng Mech 2015;141(6):04014165. https://doi.org/10.1061/(ASCE)EM.1943-7889.0000883.

[50] Foster SJ, Bailey CG, Burgess IW, Plank RJ. Experimental behaviour of concrete floor slabs at large displacements. Eng Struct 2004;26(9):1231–47.

[51] Martin T, Taylor Su, Robinson D, Cleland D. Finite element modelling of FRP strengthened restrained concrete slabs. Eng Struct 2019;187:101–19.

[52] Rankin G, Long AE. Predicting the punching strength of conventional slab-column specimens. Proc Inst Civ Eng 1987;82(2):327–46.